

2010

# Advanced Blade Testing Methods for Wind Turbines

Puneet Malhotra

*University of Massachusetts Amherst*

Follow this and additional works at: <https://scholarworks.umass.edu/theses>



Part of the [Mechanical Engineering Commons](#)

---

Malhotra, Puneet, "Advanced Blade Testing Methods for Wind Turbines" (2010). *Masters Theses 1911 - February 2014*. 529.  
Retrieved from <https://scholarworks.umass.edu/theses/529>

This thesis is brought to you for free and open access by ScholarWorks@UMass Amherst. It has been accepted for inclusion in Masters Theses 1911 - February 2014 by an authorized administrator of ScholarWorks@UMass Amherst. For more information, please contact [scholarworks@library.umass.edu](mailto:scholarworks@library.umass.edu).

**ADVANCED BLADE TESTING METHODS FOR WIND TURBINES**

A Thesis presented

by

**PUNEET MALHOTRA**

Submitted to the Graduate School of the  
University of Massachusetts Amherst in partial fulfillment  
of the requirements for the degree of

**MASTER OF SCIENCE IN MECHANICAL ENGINEERING**

September 2010

Department of Mechanical and Industrial Engineering

© Copyright by Puneet Malhotra 2010

All Rights Reserved

# ADVANCED BLADE TESTING METHODS FOR WIND TURBINES

A Thesis presented

by

PUNEET MALHOTRA

Approved as to style and content by:

---

Robert Hyers, Chair

---

James F. Manwell, Member

---

Jon McGowan, Member

---

Donald Fisher, Department Head,  
Department of Mechanical and Industrial  
Engineering

## ACKNOWLEDGEMENTS

I would like to acknowledge and express my special thanks to the following people who have encouraged and supported me throughout this entire process.

James Manwell, Robert Hyers, Jon Mc Gowan, Patrick Quinlan, Jody Lally

*University of Massachusetts, Amherst*

Jason Cotrell, Scott Hughes, Scott Lambert, Dave Simms, Darren Rahn, Cary Hertert,  
Billy Hoffman, Jason Jonkman, Cynthia Syzdlek and Walt Musial

*National Renewable Energy Laboratory*

Michael Joseph Desmond Jr.

*Embry-Riddle Aeronautical University*

## **ABSTRACT**

ADVANCED BLADE TESTING METHODS FOR WIND TURBINES

SEPTEMBER 2010

PUNEET MALHOTRA

B.E.M.E PUNJAB TECHNICAL UNIVERSITY, INDIA

M.S.M.E, UNIVERSITY OF MASSACHUSETTS AMHERST

Directed by: Professor Robert W. Hyers

This thesis consists of a detailed analysis of different blade testing methods and improvements to a novel concept for tri-axial testing of large wind turbine blades. As the blades are one of the most critical components of the wind turbine, they have to be tested in order to ensure that their specifications are consistent with the actual performance of the blade. It must be demonstrated that the blade can withstand both the ultimate loads and the fatigue loads to which the blade is expected to be subjected during its design service life. There are basically two types of blade testing: static testing and fatigue testing. Testing of the blades statically and dynamically helps in improving the designs and the manufacturing processes.

This thesis has two objectives. The first objective is to document the assumptions, calculations and results of an initial sizing of a bell crank system for testing blades 50m, 60m and 70m long. The second objective of this report is to document the modeling of one of the alternatives to bell crank system in SolidWorks. The thesis ends with conclusions and suggestions for future work.

An advanced blade testing method which can be used for large wind turbine blades is developed and so are the system requirements. The concept is used to excite the blade in flapwise and edgewise direction simultaneously. The flap motion of the blade is caused by BREX resonant technology, which is already used by National Renewable Energy Laboratory (NREL) in Colorado, and edgewise motion is delivered by the use of two inclined hydraulic actuators and linear guide rail system is used to move the inclined actuators in the flapwise direction along the blade motion. The hydraulic system and linear guide rail requirements are analyzed and discussed.

The design is discussed and analyzed in detail proving it to be feasible. The cost estimation is done for the design. It is recommended for implementation as it will serve as an efficient way of testing large wind turbine blades.

# TABLE OF CONTENTS

ACKNOWLEDGEMENTS .....	iv
ABSTRACT .....	v
LIST OF TABLES .....	ix
LIST OF FIGURES .....	x
1. BACKGROUND AND INTRODUCTION .....	1
1.1 Brief History of Wind energy .....	1
1.2 Introduction to Modern Wind Energy.....	2
1.3 Wind Turbine Blade Construction and Material.....	4
1.4 Wind and Gravity Loads .....	6
1.5 Purpose and Importance of blade Testing.....	8
1.6 Blade Testing Methods .....	8
1.6.1 Static Testing .....	9
1.6.2 Fatigue Testing.....	10
2. SCOPING OF A DUAL-AXIS, FORCED DISPLACEMENT, EDGEWISE ACTUATOR FOR TESTING 50-70m BLADES .....	16
2.1 Motivation for dual axis testing .....	16
2.2 Limitations of bell crank systems .....	17
2.2.1 Cross-coupling of flapwise and edgewise force components .....	17
2.2.2 Induced Pitch Moments .....	18
2.2.3 Pushrod sizing.....	19
2.2.4 Bell crank spanwise positioning .....	21
3. ALTERNATIVE EDGE ACTUATION DESIGNS .....	23
3.1 Actively-positioned Bell crank .....	23
3.2 NaREC's Blade-Mounted Edgewise Actuator Concept .....	24
3.3 NREL's Blade-Mounted Edgewise Actuator Concepts.....	25
4. DESIGN REQUIREMENTS .....	33
4.1 Objective .....	33
4.2 Method .....	33
4.3 Normalized blade Properties.....	33
4.3.1 Mass per unit length.....	34
4.3.2 Chord Length .....	35
4.3.3 Flap Stiffness .....	36
4.3.4 Edge Stiffness .....	37
4.3.5 Axial Stiffness.....	38
4.3.6 Torsional stiffness.....	39
4.4 Calculations & analysis.....	40
4.4.1 About MATLAB Code .....	40



4.4.2	Static Analysis (blade without saddles, under its own weight) .....	40
4.4.3	Static & dynamic analysis (blade with saddles) .....	43
4.4.3.1	Static analysis.....	45
4.4.3.2	Dynamic analysis .....	47
4.5	Hydraulic requirements .....	49
4.6	MTS Series 201 Hydraulic Actuator.....	51
4.6.1	Benefits .....	52
4.6.2	Options .....	53
4.6.3	Specifications .....	54
4.6.3.1	Rod diameter.....	55
4.6.3.2	Inner & Outer diameter of cylinder .....	55
4.7	Flange specifications.....	56
4.8	Universal Joint specifications .....	58
4.9	Linear guide rail system requirements .....	60
4.9.1	Active trolley system.....	61
4.9.2	Force to be delivered by hydraulic actuator.....	62
5.	CONCLUSION.....	64
6.	FUTURE WORK.....	66
APPENDICES		
A.	LINEAR GUIDEWAY ASSEMBLY SPECIFICATION CHART .....	67
B.	MATLAB INPUT FILES.....	71
REFERENCES	.....	73

## LIST OF TABLES

Table	Page
2.1 Deflections, pushrod length, and force components required to maintain a flapwise pushrod component less than 10% of the pushrod force [15] .....	19
2.2 Deflections, pushrod length, and force components required to maintain a pushrod force component that is less than 20% of the pushrod force [15].....	20
4.1 Static analysis (blade without saddles, under its own weight) calculations and results .....	41
4.2 Static analysis (blade with saddles) calculations and results .....	45
4.3 Dynamic analysis calculations and results.....	48
4.4 Hydraulic system requirements.....	51
4.5 Specifications of SAE single part butt weld flange .....	57
4.6 Specifications of SAE single part blind flange .....	58
4.7 Estimated specifications for a 3” bore diameter universal joint .....	59

## LIST OF FIGURES

Figure	Page
1.1 Representative size, height, and diameter of wind turbines.....	2
1.2 World cumulative installed power capacity, 1990-2008 .....	3
1.3 Typical wind turbines .....	4
1.4 Typical wind turbine blade cross-section .....	5
1.5 Blade bending moment directions .....	6
1.6 Blade bending moment forces .....	7
1.7 Static Testing using ballast weights and winches .....	9
1.8 RISØ's single-axis resonance test system.....	12
1.9 Dual-axis forced-displacement test system.....	13
1.10 BREX dual axis resonance test system.....	14
1.11 UREX dual axis resonance tests system .....	15
1.12 Schematic of the UREX Resonant Test .....	15
2.1 Schematic of the phase angle (left) and corresponding blade deflection (right) with a 70° phase angle .....	16
2.2 Schematic of forced displacement test using a bell crank system .....	17
2.3 Schematic of bell crank geometry and force component diagram when the blade cannot be cut to facilitate attachment of the pushrod.....	18
2.4 Normalized target and bell crank moment distributions for an edgewise fatigue test.....	21
3.1 Schematic of an actively-positioned bell crank system .....	24
3.2 Schematic of a blade-mounted edgewise excitation system concept.....	25
3.3 Schematic of NREL's blade-mounted edgewise excitation system concept .....	26

3.4 Alternative embodiments of NREL’s blade-mounted edgewise excitation system concepts .....	29
3.5 Design of model in SolidWorks.....	30
3.6 Model showing different types of joints .....	31
3.7 Closer view of the model .....	31
3.8 Front View of the model at different positions during the test.....	32
4.1 Mass per unit length along normalized blade station.....	34
4.2 Airfoil nomenclature showing chord length .....	35
4.3 Chord length along normalized blade station .....	35
4.4 Flap stiffness along the length of the blade .....	36
4.5 Edge stiffness along the length of the blade .....	37
4.6 Axial Stiffness along the length of the blade .....	38
4.7 Torsional stiffness along the length of the blade .....	39
4.8 Flap and edgewise mode shapes for static case (blade without saddles) .....	42
4.9 Tip deflection when the blade is stationary (without saddles, under its own weight) .....	42
4.10 Moment distribution along the length of the blade (without saddles, under its own weight).....	43
4.11 Flap and edgewise mode shapes for static case 2 (blade with saddles) .....	46
4.12 Tip deflection when the blade is stationary (with saddles on).....	46
4.13 Moment distribution along the length of the blade (with saddles) .....	47
4.14 Flap and edge deflections along the length of the blade for dynamic case.....	48
4.15 Flap and edge moments along the length of the blade for dynamic case .....	49
4.16 Angle between the actuators .....	49
4.17 MTS Series 201 Hydraulic Actuator.....	52

4.18 Actuator Specification drawing .....	54
4.19 Drawing of SAE single part butt weld flange.....	56
4.20 Drawing of SAE single part blind flange.....	57
4.21 Drawing along with 3-D preview of a universal joint .....	58
4.22 Drawing specifications for the block .....	60



**NON-DISCLOSURE AGREEMENT**  
(“Agreement”)

This Agreement is entered into by and between the Alliance for Sustainable Energy, LLC, the Manager and Operator of the National Renewable Energy Laboratory (“NREL”) under Prime Contract No. DE-AC36-08GO28308 for the U.S. Department of Energy (the “DOE”), located at 1617 Cole Boulevard, Golden, Colorado, 80401 and the University of Massachusetts, an institute of higher education of the Commonwealth of Massachusetts, as represented by its Amherst campus (“University”), whose place of business is located at Research Administration Building, 70 Butterfield Terrace, Amherst, MA 01003. Both parties are hereinafter referred to individually as the “Party,” and collectively as the “Parties”. The effective date (“Effective Date”) of this Agreement shall be the signature date of the last of the Parties to sign this Agreement.

1. PURPOSE

- a. NREL wishes to provide to University, for a period of 12 months, and University wishes to obtain access to NREL PROTECTED INFORMATION relating to ROI No. PROV/09-02, Serial No. 61/161,606 titled “Blade-Mounted Tri-Axial, Blade Actuation Systems and Methods” which NREL considers NREL PROTECTED INFORMATION. NREL is furnishing NREL PROTECTED INFORMATION to University to permit University to assess and develop the technology for a graduate student’s thesis, which may be published during the term of this Agreement.
- b. As used herein, NREL PROTECTED INFORMATION means information generated in the performance of, or pursuant to the performance of the Prime Contract regardless of form or characteristic, (including but not limited to technical data, microorganisms, computer software, drawings, photographs, process information, samples, equipment, specifications, and the like) which would be proprietary information had it been generated by a non-federal entity third party, and which can be restricted from dissemination by the Bayh-Dole Act, 35 U.S.C. §200 et seq, other applicable laws, or DOE rules or regulations.

2. PROPRIETARY INFORMATION

- a. University agrees to use NREL PROTECTED INFORMATION only for the purpose(s) set forth in Paragraph 1.a. above. University will treat all NREL PROTECTED INFORMATION disclosed to University by NREL, whether such original disclosure is written or oral, as confidential and proprietary. However, oral disclosure of information (i.e., information expressed by spoken words) to University by NREL shall be considered NREL PROTECTED INFORMATION only upon being identified as such at the time of disclosure, reduced to writing, and a copy of it provided by NREL to University within thirty (30) days of the oral disclosure. Except in the context of a publication as described in Paragraph 1.a. above, University will not disclose NREL PROTECTED INFORMATION to any third party, except the DOE, for a period of five (5) years from the Effective Date of this Agreement.
- b. All NREL PROTECTED INFORMATION will be identified and marked by NREL as “NREL PROTECTED INFORMATION” at the time it is conveyed to University except for oral disclosures of NREL PROTECTED INFORMATION as noted in Paragraph 2.a. above.
- c. University agrees that access to NREL PROTECTED INFORMATION will be provided only to University’s employees, agents and independent contractors who are required to have access specifically related to the uses permitted herein and to the DOE. University further agrees that it will inform individuals having access to NREL PROTECTED INFORMATION of the confidential nature of the NREL PROTECTED INFORMATION and restrictions on its publication, disclosure and use and shall assume the responsibility that such employees and independent contractors will

Unilateral (OUT) Non-Disclosure Agreement Template

preserve the secrecy of such information with respect to third parties.

- d. The obligations of confidentiality set forth in this Agreement do not apply to information which: (i) is generally known or available from the DOE or other sources without obligation concerning its confidentiality; (ii) has been made available by NREL to the DOE, University, or others without obligation concerning its confidentiality; (iii) is already in the possession of University without obligation concerning its confidentiality or (iv) is required to be disclosed by law, including a court order from a court of competent jurisdiction.

3. MISCELLANEOUS


- a. It is further agreed that disclosure of NREL PROTECTED INFORMATION to University shall not constitute any grant, option, or license under any patent or other rights now or hereinafter held by NREL.
- b. If not earlier terminated by either party, this Agreement will expire twelve (12) months after the last party signs this Agreement.
- c. As appropriate, either party may terminate this Agreement with or without cause by giving the other party thirty (30) days' prior written notice.
- d. Upon expiration or termination of this Agreement University will within two (2) weeks of written request from NREL return all documents concerning the NREL PROTECTED INFORMATION to the NREL and all copies of any such documents or certify in writing their destruction, subject to University's right to retain one copy of each such document in the files of its law department or outside legal counsel for record purposes only.
- e. Notwithstanding the above, the obligations of confidentiality set forth in Paragraph 2, herein, will survive termination of this Agreement.
- f. A party receiving NREL PROTECTED INFORMATION shall adhere to U.S. Export Administration Laws and Regulations and shall not export or re-export any such NREL PROTECTED INFORMATION, any technical data, items or products arising from the information to any country or person unless properly authorized by the U.S. Government.
- g. The parties acknowledge that this Agreement may be executed in a number of counterparts and the sum of said counterparts shall represent a fully executed document. The parties further acknowledge that facsimile signatures are fully binding and constitute a legal method of executing this Agreement.

AGREED:

ALLIANCE FOR SUSTAINABLE ENERGY, LLC

UNIVERSITY OF MASSACHUSETTS

By: 

By: 

Name: Casey Porto

Name: Nicholas DeCristofaro, Ph.D.

Title: Sr. Vice President

Title: Director Commercial Ventures & Intellectual Property

Date: 3-30-09

Date: 3-30-09

## CHAPTER 1

### BACKGROUND AND INTRODUCTION

This chapter provides the background information on the research that was conducted throughout the course of this study. An introduction is given on the objectives of this research and its importance. Additionally, an overview of the study that was conducted is provided.

#### **1.1 Brief History of Wind energy**

The purpose of the research conducted for this project is the advancement of the knowledge and capabilities in the area of wind turbine blade testing. Prior to the discussion of different blade testing methods, an introduction to current wind energy technology and its history will be presented.

The re-emergence of the wind as a significant source of the world's energy must rank as one of the significant developments of the late 20<sup>th</sup> century. The first windmills on record were built by Persians around 900 A.D [1]. These vertical axis windmills were not very efficient at capturing the wind's power and were particularly susceptible to damage during high winds. During the Middle Ages, wind turbines began to appear in Europe [2-4]. These turbines resembled the 4-bladed horizontal axis windmill typically associated with Holland. The applications of windmills in Europe included water pumping, grinding grain, sawing wood and powering tools. Like modern wind turbines, the early European systems had a yaw degree of freedom that allowed the turbine to turn into the wind to capture the most power. The use of windmills in Europe reached their height in the 19th century just before the onset of the Industrial Revolution. At this time, windmill designs were beginning to include some of the same features found on modern



wind turbines including yaw drive systems, air foil shaped blades and a power limiting control systems [5-7].

Wind turbines have continued to evolve over the past 20 years and the overall cost of energy required to produce electricity from wind is now competitive with traditional fossil fuel energy sources [8-9]. This reduction in wind energy cost is the result of improved aerodynamic designs, advanced materials, improved power electronics, advanced control strategies and rigorous component testing.

### 1.2 Introduction to Modern Wind Energy

Over the last 25 years, wind turbines have evolved and are now cost competitive with traditional energy sources in many locations. The size of the largest commercial wind turbines, as illustrated in Figure 1.1, has increased from approximately 50 kW to 2 MW, with machines up to 5 MW under design [1].

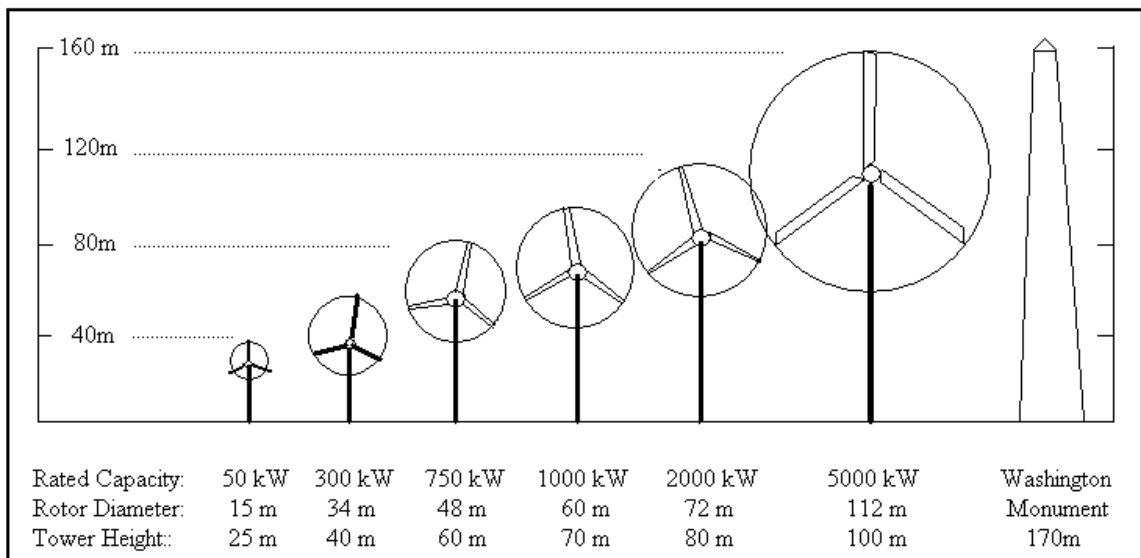


**Figure 1.1 Representative size, height, and diameter of wind turbines**

Wind turbine technology, dormant for many years, awoke at the end of 20<sup>th</sup> century to a world of new opportunities. Developments in many other areas of technology were adapted to wind turbines and have helped to hasten their re-emergence. A few of many areas which have contributed to the new generation of wind turbines include materials science, computer science, aerodynamics, analytical methods, testing, and power electronics. The total installed capacity in the world as of year 2005, as shown in Figure 1.2 [11], was approximately 60,000 MW, with majority of installations in Europe. Offshore wind energy systems are also under active development in Europe. Design standards and machine certification procedures have been established, so that the reliability and performance are far superior to those of 1970s and 1980s. The cost of energy from wind has dropped to the point that in some sites it is competitive with conventional sources, even without incentives. In those countries where incentives are in place, the rate of development is strong [1].

Global Cumulative Installed Wind Power Capacity, 1990-2008

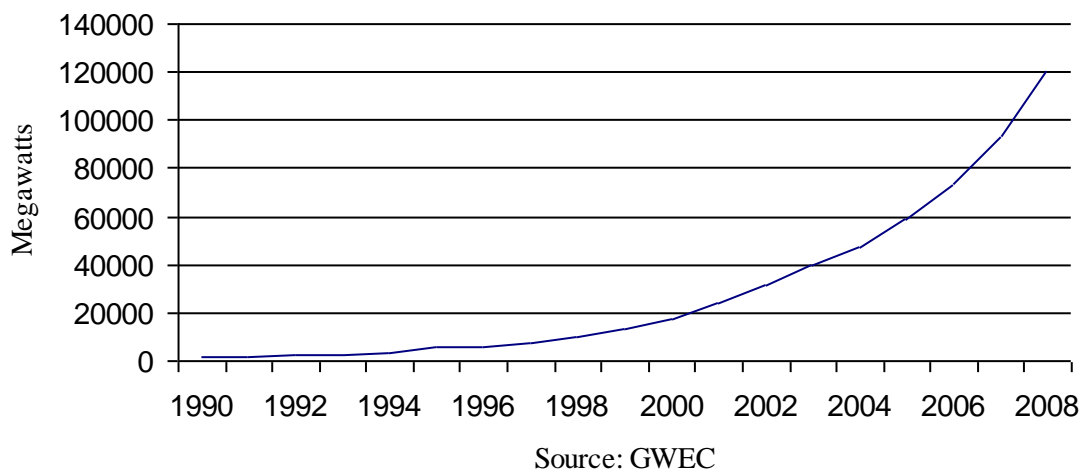


Figure 1.2 World cumulative installed power capacity, 1990-2008



**Figure 1.3 Typical wind turbines**

Like the 1.5 MW turbine shown in Figure 1.3 [12], most turbines have a horizontally mounted hub with two or three blades. As the blades become longer to capture more power, the static and dynamic loads on the blades and other components increase. In general, a blade for a 1.5-MW turbine is 34 meters in length or greater and weighs as much as 6,000 Kg (13,200 lbs) [10].

### **1.3 Wind Turbine Blade Construction and Material**

Blades are designed with a circular root which transitions into an airfoil with the maximum chord occurring at about 25% span. A typical wind turbine blade cross-section is shown in Figure 1.4. Most wind turbine blades are fabricated using reinforced fiberglass composite materials with epoxy or vinyl ester matrices. Single or double shear webs are usually combined with planks of unidirectional laminates to form integral I-

beam or box beam structures that carry the loads along the blade's span. Foam or balsa sandwich construction is also used for wide panels to prevent buckling instabilities [10].

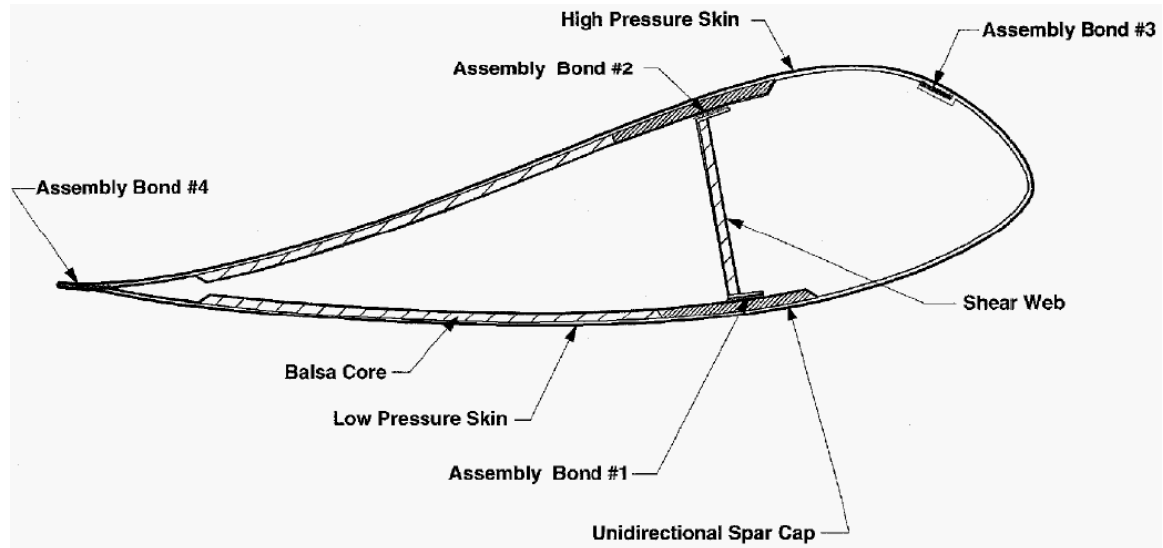


**Figure 1.4 Typical wind turbine blade cross-section**

Several fabrication processes are used which include resin infusion, prepreg, and vacuum-assisted resin transfer molding processes. The blade structure transmits aerodynamic and inertial forces along the span into a steel hub which connects to the rotating drive system. As blades grow longer, power production increases with the swept area of the rotor disc, or by the square of the blade length. All other things being equal, the mass of the blade will increase by the cube of the blade length. Continuous improvements in manufacturing methods have kept the rate of increase of mass somewhat lower than that, but mass still increases faster than the power output. If the trend towards larger rotors and longer blades is to continue, further innovations in materials (e.g. carbon fiber), manufacturing, and load-relieving designs must be introduced to reduce weight. All these innovations require blade testing validation [10].

## 1.4 Wind and Gravity Loads

Wind turbine blades are among the most critical components of a wind turbine and thus need special attention on their testing by determining the actual load experienced during its operation. Blades are primarily subjected to two types of loads: aerodynamic loads such as shear, drag, lift, etc., and inertial loads such as gravity, blade dynamics, etc. These forces generally occur in orthogonal bending directions: flap and lead-lag, as shown in Figure 1.5. The relative angle between the airfoil chord and plane of rotation varies radially along the blade length. Since the blade travels in a circle, the tangential speed of the blade varies radially along the blade and twist angle varies to control the relative angle of attack [10].

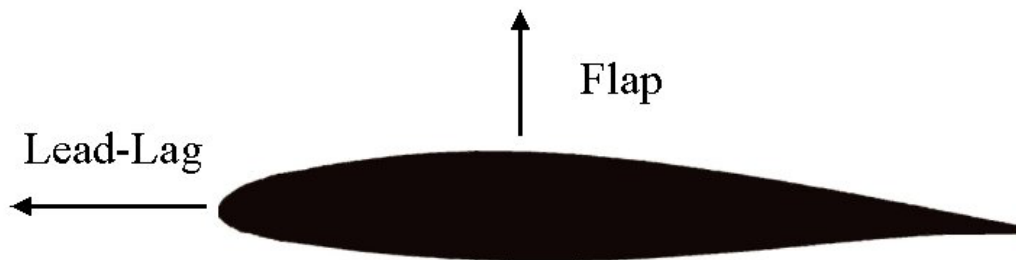


**Figure 1.5 Blade bending moment directions**

The most significant blade bending moments induced by wind loads typically occur in flapwise direction. Flapwise forces have stochastic and deterministic components. The stochastic component is due to variability in wind speed and direction, and turbulence from nearby objects. The deterministic component is invariant, and increases with height in accordance to boundary layer characterization.

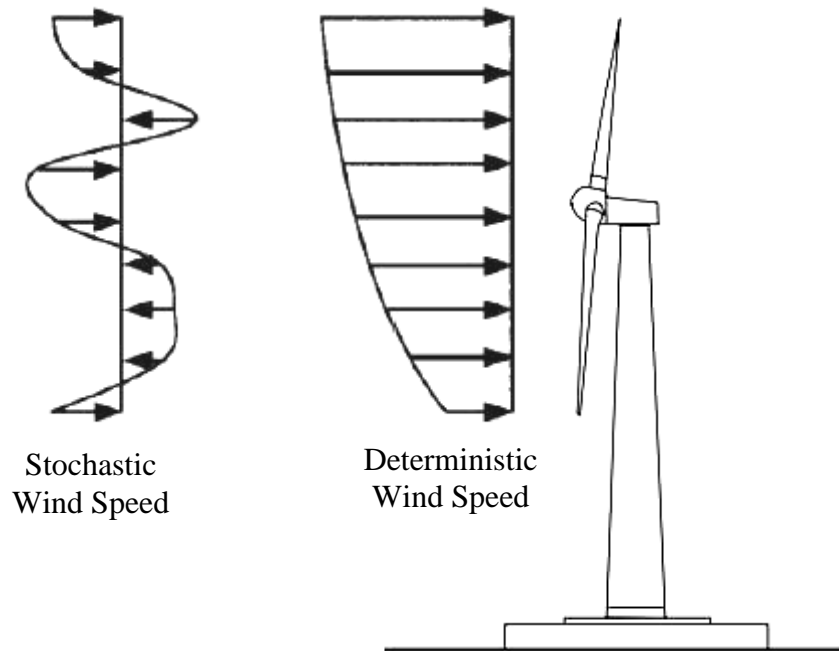


**Figure 1.6 Blade bending moment forces**

For smaller blades, gravity loads were not considered a major source of fatigue. But, as the size of blades has gotten larger and heavier, the effects of gravity cannot be ignored. Gravity forces and generator torques results in lead-lag forces. Blade loads in this direction have a larger deterministic component. Because of the airfoil shape, wind turbine blades are typically very stiff in the lead-lag direction and higher bending moments in the outboard sections are very large in this direction as compared to flap bending moments [10].

Since both flap and lead-lag loads are cyclic in nature, fatigue stress is the primary factor for the failure of the component, as in the wings of an airplane. While there are accurate fatigue testing methods in the aviation industry, budget constraints have eliminated the direct application into the wind industry. However, alternate testing methods have been developed at many laboratories over the world, where the loads are

applied to test the blades statically and dynamically to ensure that it will behave as expected when exposed to extreme conditions, like hurricane and high-speed gusts.

### **1.5 Purpose and Importance of blade Testing**

Because the blades are among the most critical components of the wind turbine, they have to be tested in order to ensure that their specifications are consistent with the actual performance of the blade. According to the International Electrotechnical Commission (IEC) report, TS 61400 pt 23, the fundamental purpose of a wind turbine blade test is to demonstrate to a reasonable level of certainty that a blade type, when manufactured according to a certain set of specifications, has the prescribed reliability with reference to specific limit states, or, more precisely, to verify that the specified limit states are not reached and the blades therefore possess the strength and service life provided for in the design [13]. It must be demonstrated that the blade can withstand both the ultimate loads and the fatigue loads to which the blade is expected to be subjected during its designed service life. In other words, the blade should not fail before the end of its expected service life. Testing of the blades statically and dynamically helps in improving the designs and the manufacturing processes, which further helps in progress of the wind industry as a whole. In field, the blades are typically subjected to normal operating conditions only. Such testing does not ensure that the blade can withstand extreme operating conditions.

### **1.6 Blade Testing Methods**

Generally, the blade testing methods fall into two main categories, static testing and fatigue testing of the blade. The test load can either be load-based or strength-based.

The purpose of the load-based test is to show that the blade will sustain the intended loads without failure, and is normally used as part of a certification process. This type of testing is performed to demonstrate that the tested blade, within a certain level of confidence, has met the structural design requirements with respect to its normal operating or extreme load conditions. Strength based testing uses as-manufactured blade strength data as its basis and blades are tested to failure. This allows a direct verification of the blade strength, and an assessment of ways in which the design computations, and the resulting design itself, might be improved. This method can be used to find the lowest strength location, relative to expected strength, within a broad region.

### **1.6.1 Static Testing**

In static testing, loads are applied to the blade statically in one direction to establish its ultimate strength. This type of test can either be intentionally destructive or non-destructive. This type of testing is done with the purpose of predicting a blade's ability to withstand extreme loads such as those caused by hurricane wind forces or unusual transient conditions, in order to determine the ultimate strength of the blade.



**Figure 1.7 Static Testing using ballast weights and winches**



Static testing is accomplished in a number of ways. The most common of these uses electric winch system, due to ease of controlling it. Hydraulic actuators have also been used in the past but large displacements in longer blades make them an expensive option. Other way of performing a static test is to hang ballast weights from the blade at specified locations. In case of larger blades, the blade is attached to the test stand at an angle in order to prevent the tip of the blade from touching the ground, as shown in Figure 1.7 [14] above.

### **1.6.2 Fatigue Testing**

This type of test is mainly used to identify structural defects inherent in either the design or manufacturing process. Fatigue tests are performed to verify the durability of the blade, with a sinusoidal loading profile. Fatigue tests apply a loading spectrum which may contain a 1 million to 5 million load cycles. It is typically performed in two primary directions, flap and lead-lag. The magnitude of the static loading is almost always higher than the fatigue loading. Blades can be fatigue tested sequentially, first in the edgewise direction followed by testing in the flapwise direction. Dual-axis testing is another approach. Here, both flap and lead-lag loads are applied simultaneously. Dual-axis testing can in principle, better simulate loads experienced in the field and can result in shorter overall test duration. Currently, there are two methods used to apply these loads to the blade; these are generally referred to as forced displacement and resonant oscillation testing.

Forced displacement testing uses long stroke actuators or bell cranks and push rods to force the blade to a prescribed displacement. This is done in a cyclic manner and

has the benefit of being able to apply nearly any combination or sequence of loading cycles to the blade. In general this type of loading works well for edgewise testing where the loads are closer to fully reversed bending than in flap. However, in the flap direction forced displacement testing requires very long stroke actuators and high forces, which results in very high hydraulic flow rate requirements for large blades. Resonant testing uses an oscillating mass driven by an actuator attached to the blade through a frame.

There are few laboratories throughout the world that have the facility to perform static and fatigue testing of the wind turbine blades; RISØ National Laboratories in Denmark, the Center for Renewable energy and Sources (CRESES) in Greece, the Wind turbine Materials and Constructions Knowledge Center (WMC) at TU Delft in Netherlands, National Renewable energy Laboratories (NREL) in US, New and Renewable Energy Centre (NaREC) in United Kingdom and LM glasfiber in-house testing facility located in Lunderskov, Denmark. In United States, other two large blade test facilities namely, Massachusetts Wind Technology Testing Centre (WTTC) in Charlestown, MA and the Large Blade Test Facility in Houston, Texas are under construction. Each of these test facilities has independently developed blade testing methods. RISØ performs fatigue tests by applying cyclical loads in either the flap or lead-lag direction using an electric motor that rotates an eccentric mass, as shown in Figure 1.8 [10]. This testing method is referred to as the single-axis resonance test. Single axis resonance test applies each component independently in two separate tests, thus making it less accurate for predicting life of the blade as it does not simulate the actual loading conditions experienced in the field. However, it has several advantages over dual-axis forced-displacement test. By adding masses to the blade, it is possible to match the

bending moment distribution in the flap or lead-lag direction more closely approximate the bending moments experienced in service, for this test. While the added masses lower the system's natural frequency, test cycle frequency remains higher than forced-displacement test. Dual axis testing is limited by hydraulic supply and hence takes less time to accumulate a specific number of cycles, making it possible to complete fatigue test faster and to complete more tests per year.



**Figure 1.8 RISØ's single-axis resonance test system**

NREL, CRES and WMC use hydraulic actuators that apply loads at a single spanwise station on the blade in both flap and lead-lag directions [10]. This testing technique is referred to as dual-axis forced-displacement method. This method employs a servo-hydraulic system with actuators to exercise the blade in flap and lead-lag directions, at frequencies well below the blade's first fundamental flap natural frequency, as shown in Figure 1.9 [10]. The main advantage of this system is that the bi-axial loading creates strain profiles that more accurately agree with the service or operating conditions, as compared to single-axis tests.



**Figure 1.9 Dual-axis forced-displacement test system**

While this method is more accurate, it has several drawbacks. The forced loading system requires large forces and displacements from the hydraulic actuators. As a result, new actuators have to be designed and built each time a larger blade is used. As the actuator size increases, the hydraulic pumping requirements also increase. Accordingly, substantial equipments costs are incurred when increasing the capability of testing larger blades [10].

As the blades continued to grow larger in size, a new method was required to be developed to test the blades, keeping the costs down and to allow wind industry to compete in the energy market. This led to the development of dual-axis blade resonance excitation system (BRES). In this testing method, a small hydraulic actuator is used to displace a specified mass to excite the blade at its natural frequency in the flapwise

direction, while a bell crank system is used to provide displacement in the lead-lag direction, as shown in Figure 1.10



**Figure 1.10 BREX dual axis resonance test system**

This testing methodology has the advantage of reduced hydraulic forces in both directions and being a universal testing device for the flapwise direction. The main drawback of this system is the bell crank mechanism, as it applies a point load in the lead-lag direction using a hydraulic actuator. Advancement on this system is the dual-axis universal resonance excitation (UREX) test method. In this method, bell crank mechanism is replaced by independent hydraulic actuators and masses in the saddle device, which resonates the blade in both flap and lead-lag directions, as shown in Figure 1.11





**Figure 1.11 UREX dual axis resonance tests system (photo taken at NWTC, NREL)**

This system was tested on a small scale and proved to be a valid test method. Future work and tests are currently underway to refine and scale the system to provide a universal mechanism that can be used for any size blade.

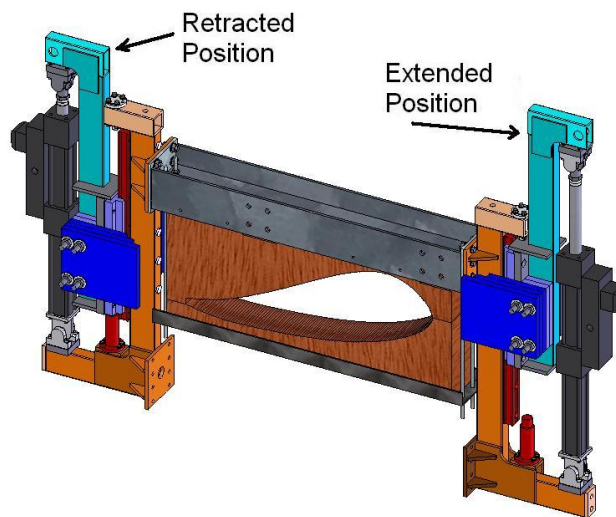


**Figure 1.12 Schematic of the UREX Resonant Test**

## CHAPTER 2

### SCOPING OF A DUAL-AXIS, FORCED DISPLACEMENT, EDGEWISE

#### ACTUATOR FOR TESTING 50-70M BLADES

##### 2.1 Motivation for dual axis testing

Fatigue testing of the blades can be done sequentially, first in the edgewise direction followed by testing in the flapwise direction. This is termed as single axis testing. Dual axis testing is another method of testing blades. In this case, both the flap and edgewise loads are applied simultaneously. This type of approach for testing the blades is preferred over single axis testing as it simulates the actual blade loads experienced in the field by including the phase angle between flapwise and edgewise loads. Moreover, dual axis testing results in a shorter overall duration for testing the blades. The phase angle between the flapwise and edgewise forces is defined as the angular change in the rotor between the maximum flap bending moment and the maximum lead-lag bending moment over a single rotation as shown in Figure 2.1

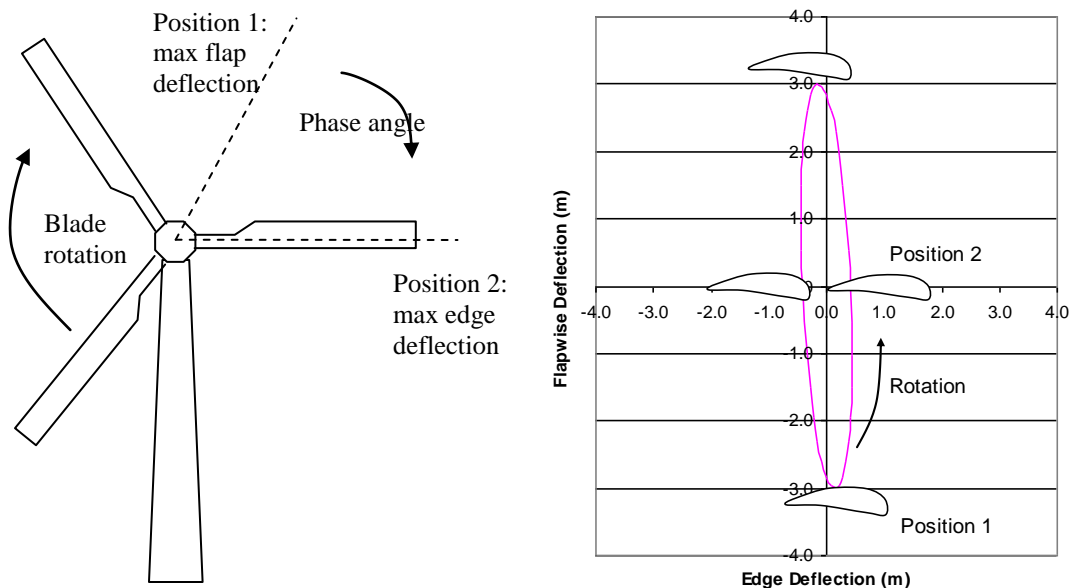


**Figure 2.1 Schematic of the phase angle (left) and corresponding blade deflection (right) with a 70° phase angle**

## 2.2 Limitations of bell crank systems

A schematic of a forced displacement test using a bell crank system is shown in Figure 2.2. Ideally, a bell crank system should impart the force only in edgewise direction even when the flapwise deflection is occurring. However, the system imparts an additional force as discussed below.

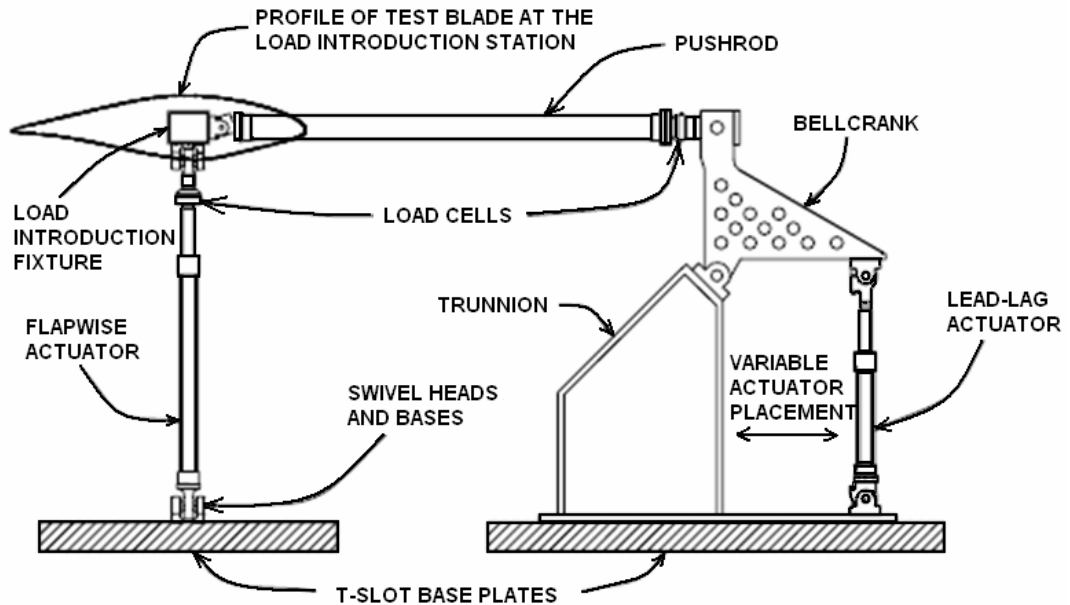


**Figure 2.2 Schematic of forced displacement test using a bell crank system**

### 2.2.1 Cross-coupling of flapwise and edgewise force components

As shown cross coupling is the effect of flapwise force being introduced due to edgewise actuator, or edgewise load component introduced by flapwise actuator. Flapwise and edgewise force components are shown in Figure 2.3. This cross-coupling requires correction factors to be incorporated into the whole testing mechanism.



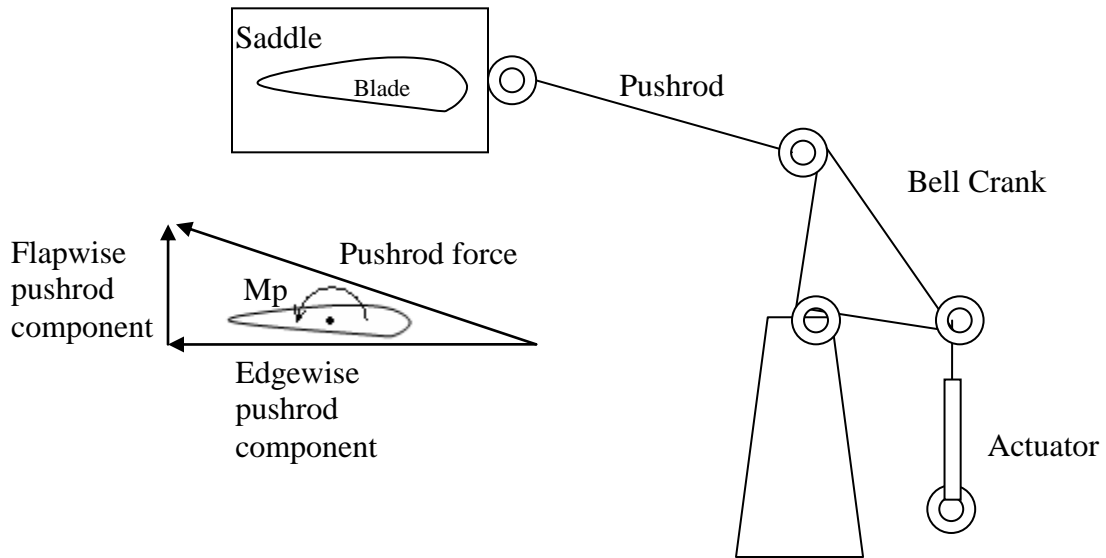


**Figure 2.3 Schematic of bell crank geometry and force component diagram when the blade cannot be cut to facilitate attachment of the pushrod**

### 2.2.2 Induced Pitch Moments

As shown in Figure 2.2, the pushrod is connected to the blade on the pitch axis. As the blade cannot be cut, the pushrod must be attached to the front of the blade. In this case, the flapwise component of the pushrod force creates an undesirable pitching moment. Keeping the concern with floor space requirements for a large blade test facility, every effort has to be made to keep the pushrod length, as short as possible. On the other hand, a short push rod results in larger pushrod angles and a larger flapwise component, thereby exacerbating the pitch moments and deflections. These undesired pitch moments and deflections may result in unrealistic load conditions thus not simulating the actual load conditions, which are not acceptable to the blade manufacturers. Also, it will result in flapwise deflection at an undesired frequency resulting in non-sinusoidal waveform. For these reasons, the pushrod has to be made longer. However, building and cost a constraint comes into play and force a compromise solution.

In order to formulate the pushrod sizing, we need to know the acceptable pitch moment which is expected to vary between blade manufacturers and blade designs. One approach for sizing the pushrod length that could be considered a reasonable compromise is to size the pushrod such that the undesirable flapwise force component as shown in Figure 2.3 is less than 10% of the total pushrod force. At NREL, we estimated the pushrod length necessary to meet this constraint. The calculations assume a simplified bell crank geometry with a pushrod initial height aligned with the blade deflection.

**Table 2.1 Deflections, pushrod length, and force components required to maintain a flapwise pushrod component less than 10% of the pushrod force [15]**

<b>Blade Length (m)</b>	50	60	70	70
Phase angle (deg)	90	90	90	70
Flap Deflection (m) (2x Amplitude)	3.5	4.5	6.0	6.0
Edge Deflection (m) (2x Amplitude)	0.5	0.7	0.9	0.9
Pushrod Length (m)	18	23	30	30
Max pushrod force (metric tons)	13	23	37	37
Max flapwise pushrod component (metric tons)	0.7	1.1	1.8	2.5

In general, the length of the pushrod must be approximately 5 times the flapwise deflection at the 70% station in order to meet the 10% constraint on the vertical pushrod force component.

### 2.2.3 Pushrod sizing

The length of the push rod required to maintain a flapwise force of less than 10% of the pushrod force for a 70m blade is 30m. A 30m long push rod subject to 37 tons of force must be very large and heavy to avoid buckling. To avoid Euler buckling with a

safety factor of 4.0, the pushrod for this blade will be approximately .45m (18”) in diameter with a .019m (.75”) wall and weigh 6 metric tons. In addition, such a long pushrod would interfere with testing in the two adjacent bays. One way to reduce the length, weight, and cost of such a long pushrod is to relax the constraint to maintain a flapwise pushrod force component less than 10% of the pushrod force.

lists the reduced pushrod requirements if the constraint is relaxed to 20%. In this case, the pushrod length could be reduced in half and diameter could be reduced to (.308m) 12” with the same wall thickness thereby reducing the mass to 2 metric tons. However, the induced pitch moment and increased coupling induced by the nearly doubled flapwise pushrod load component (5 tons) may not be acceptable to the customer.

**Table 2.2 Deflections, pushrod length, and force components required to maintain a pushrod force component that is less than 20% of the pushrod force [15]**

<b>Blade Length (m)</b>	50	60	70	70
Phase angle (deg)	90	90	90	70
Flap Deflection (m) (2x Amplitude)	3.5	4.5	6.0	6.0
Edge Deflection (m) (2x Amplitude)	0.5	0.7	0.9	0.9
Pushrod Length (m)	9	11	15	15
Max pushrod force (metric tons)	13	23	37	37
Max flapwise pushrod component (metric tons)	1.3	2.3	3.6	4.9

## 2.2.4 Bell crank spanwise positioning

One alternative to reducing the space and mass requirements of a bell crank is to place the bell crank closer to the root where the flapwise deflections are smaller. However positioning the bell crank closer to the root alters the targeted moment distribution of the test.

The area of interest in a fatigue test is approximately 20% to 50% of the blade span. All calculations in this report assume the bell crank is positioned at 70% span. By positioning the bell crank at approximately 70% span location, a reasonable approximation of the target edgewise bending moment distribution can be obtained as shown in Figure 2.4 [15].

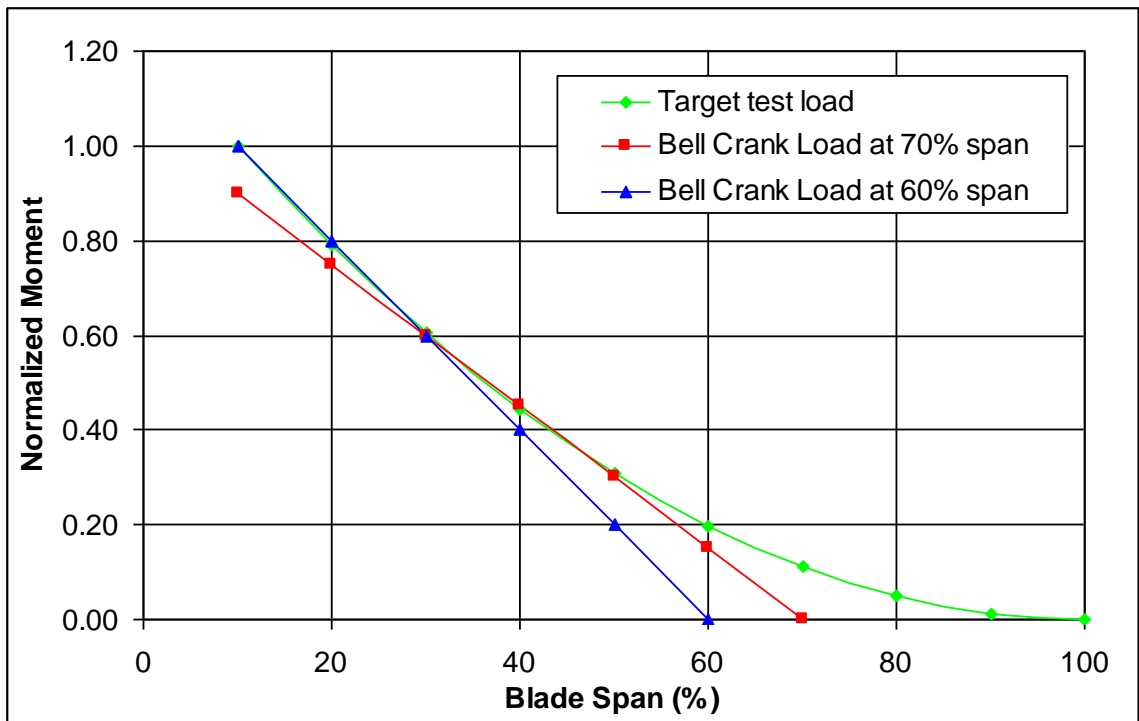


**Figure 2.4 Normalized target and bell crank moment distributions for an edgewise fatigue test**

Positioning the bell crank closer to the root (i.e. 60% span) better matches the target test load inboard but will insufficiently load the outboard sections of interest. In

addition, the pushrod must apply more force when positioned inboard but at a smaller displacement. Positioning the bell crank more outboard will have the opposite effects.

Multiple edgewise actuators would result in a closer match to the target moment distribution, but will increase the complexity of the test substantially as coordinating the forced displacement edgewise deflections of the actuators is expected to be challenging.

## CHAPTER 3

### ALTERNATIVE EDGE ACTUATION DESIGNS

Alternative bell crank designs may reduce the space and cost of the traditional bell crank system. In addition, an alternative design may facilitate tri-axial testing of wind turbine blades by enabling the control of pitch degree of freedom. In this chapter, several bell crank system configurations have been considered. The two most promising use either a blade-mounted actuator or an Actively-positioned Bell Crank (ABC).

#### 3.1 Actively-positioned Bell crank

An Actively-positioned Bell Crank (Figure 3.1) could possibly eliminate the problem caused by induced pitch moments and possibly reduce the amount of spanwise and edgewise coupling. An actively-positioned bell crank uses a second actuator to actively position a trolley to control the amount of pitch induced into the blade. If it is desired to minimize the pitch induced into the blade, the trolley is positioned to align the pushrod with the pitch axis. Additionally the flap-edge coupling could be slightly reduced as the motion of the trolley could be used to reduce the inclination angle of the pushrod. By reducing the pitch moment and coupling forces, a shorter, lighter pushrod can be used in the system. In addition, active control of the pitch moment could facilitate more accurate simulation of the operating conditions observed in the field by facilitating tri-axial testing (flapwise, edgewise, and pitch) [16].

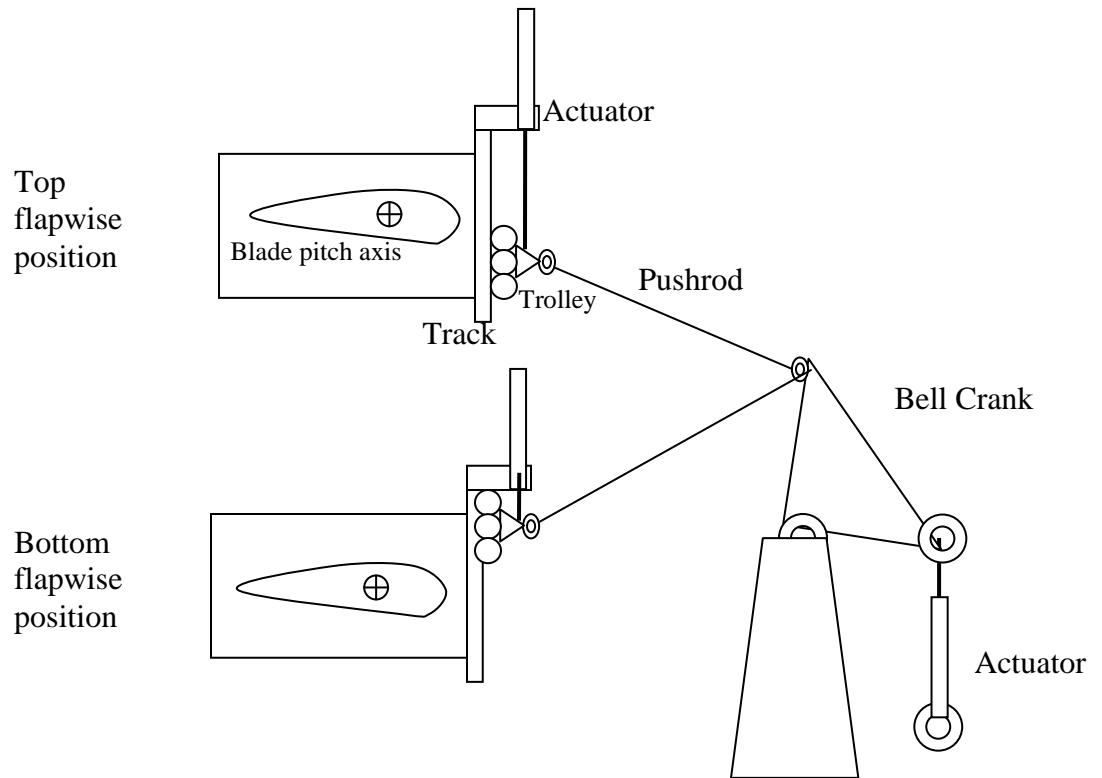


**Figure 3.1 Schematic of an actively-positioned bell crank system**

The Actively-positioned Bell Crank (ABC) will require a moderate amount of development that includes system modeling, design work, fabrication, and testing on a small to medium sized blade. The configuration is only a moderate deviation from the proven NREL bell crank system and the NREL bell crank system could be used for prototyping. This work is anticipated to take 6 months to several years depending on the resources allocated and unanticipated challenges encountered. Exploring the merits and challenges of tri-axial fatigue testing is expected to take several years [16].

### **3.2 NaREC's Blade-Mounted Edgewise Actuator Concept**

The Blade Mounted Edge Actuator system displayed in Figure 3.2 was considered by NREL and its CRADA partner NaREC in 2005. The system uses an actuator mounted on the blade and a trolley to maintain a horizontal edgewise force. This system minimizes

the coupling and dramatically reduces the amount of building space required for dual-axis testing by replacing the pushrod with an actuator. However, there is still significant pitch excitation as the actuator is offset from the pitch axis. Furthermore, rigidly mounting the actuator to the blade saddle results in bending moments being applied to the actuator piston, resulting from the saddle rotation about the test stand's horizontal and vertical axes. These bending moments are likely to damage the actuator and apply undesirable moments to the blade saddle [16].

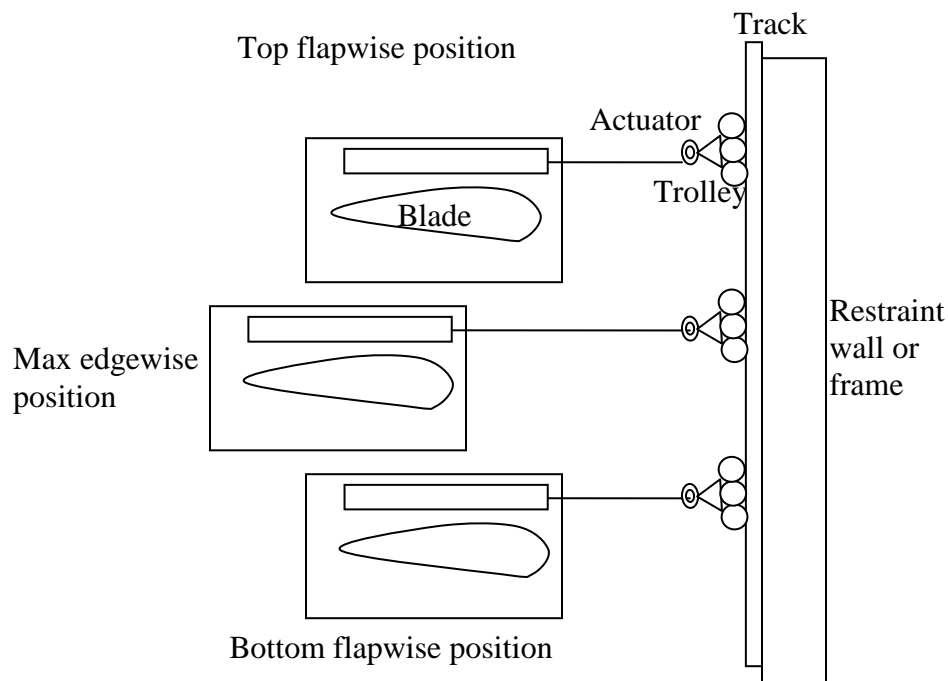


**Figure 3.2 Schematic of a blade-mounted edgewise excitation system concept**

### **3.3 NREL's Blade-Mounted Edgewise Actuator Concepts**

An improvement to NaREC's Blade-Mounted Edgewise Actuator Concept is to use two edgewise actuators on the top and bottom of the blade as shown in Figure 3.2. Using two actuators symmetrically positioned about the pitch axis dramatically reduces or eliminates the pitch moment and can even facilitate active control of the pitch moment



for tri-axial testing (deflection in the flap, edge, and pitch directions). A second benefit is that each actuator is mounted with a universal joint at each end thereby eliminating the bending forces due to the rotations of the saddle. A third benefit is that using two actuators reduces the size of the actuator. Horizontal mounting of very heavy (80 to 100 kip ~ 356 to 445 kN) actuators is believed by NREL to result in premature damage to the actuator seals and bearings [16].

The trolley's vertical position must be actively controlled using some sort of trolley positioner. Otherwise, the system behaves like a four-bar-linkage and the trolley will not stay aligned with the blade. The vertical control of the trolley could be achieved by adding a motor to the trolley or by adding a long stroke actuator as in Figure 3.3.

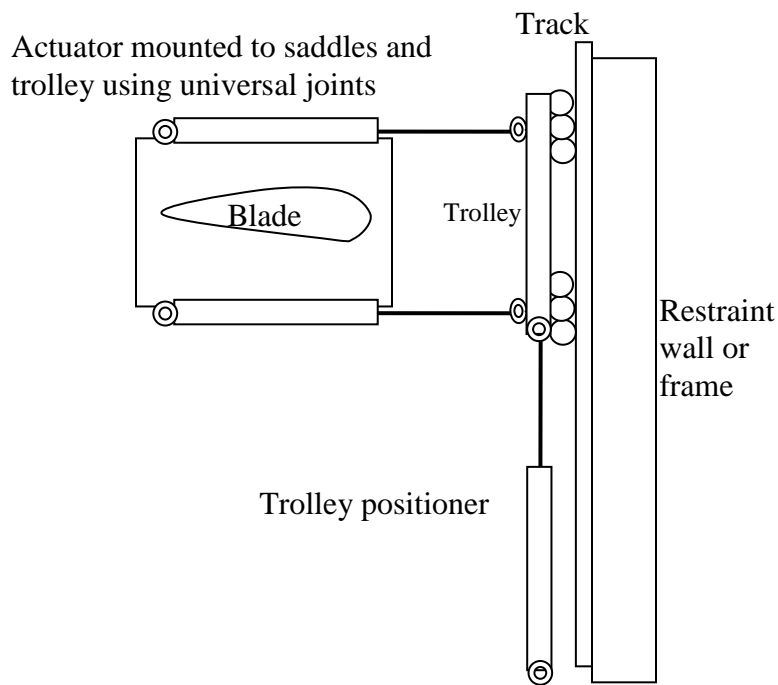


**Figure 3.3 Schematic of NREL's blade-mounted edgewise excitation system concept**

One alternative embodiment of NREL's blade-mounted edgewise excitation system concept is to mount the body of the actuators on the trolley as shown in Figure 3.4 (embodiment 1). Trolley mounted actuators will slightly reduce the mass mounted on the blade and provide an alternative means of routing hydraulic lines [16].

A second alternative (embodiment 2), as can be seen in Figure 3.4, is to use a single actuator to reduce the complexity of the system by eliminating one of the actuators. However, if tri-axial testing is desired, this solution significantly complicates the control system and would result in coupling of the flapwise and edgewise loads. In addition, a single actuator will be significantly more massive and will have to be sized to apply the entire edgewise force. This large actuator could be more sensitive to horizontal mounting [16].

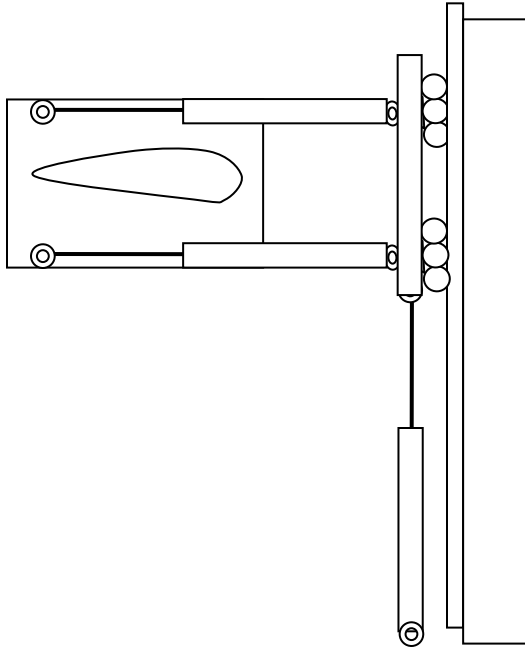
A third alternative is to use a passive trolley positioning system to simplify the system and reduce the shear loads on the edgewise actuators (embodiment 3). In this alternative, the complexity is reduced by eliminating the need to actively control the vertical position at the expense of adding a passive positioner that may be difficult to design to allow all the desired degrees of freedom [16].

A fourth alternative (embodiment 4) is an improvement over the alternatives previously mentioned above in this report. This design uses a passive trolley system with two inclined edgewise actuators on the top and bottom of the blade, mounted via universal joints or other configurations that result in similar degrees of freedom. The inclined orientation converts a large portion of actuator bending load to actuator axial loads, thereby increasing seal life and service interval. Furthermore, the use of two actuators which tend to be more forgiving of horizontal or near-horizontal positioning.

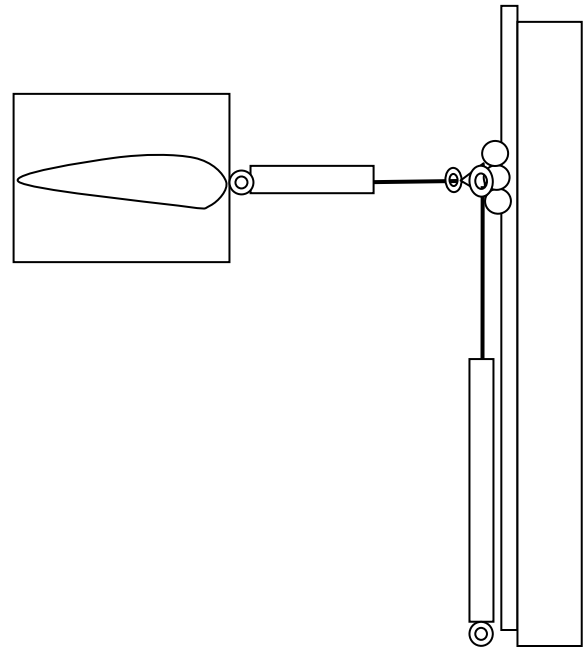
The inclined actuator system is lighter and more easily controlled than the other embodiments facilitating the possible use of multiple actuator systems along the span of the blade. Perhaps most importantly, using two inclined actuators allows the blade to be significantly closer to the trolley rail, proportionally reducing pitch moments imparted by the system mass and trolley friction [16].

This research will focus on improving current component testing methods. This project will help to reduce the cost required to produce energy from wind by improving upon current testing methods and introducing a test loading method to properly perform fatigue testing of wind turbine blades. Additionally, the research conducted for this project will make it feasible and more economical to test the next generation of wind turbine blades.

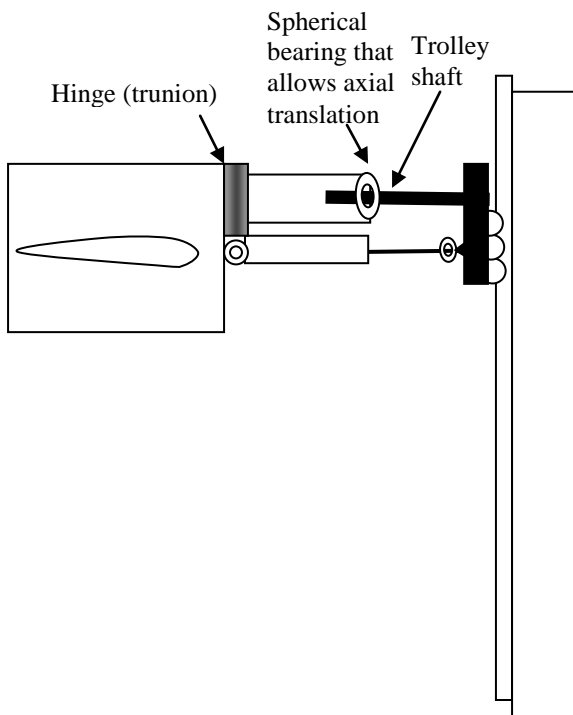
**Alternative Embodiment 1  
(Trolley mounted actuators)**



**Alternative Embodiment 2  
(Single Actuator)**



**Alternative Embodiment 3  
(passive link)**



**Alternative Embodiment 4  
(inclined actuators)**

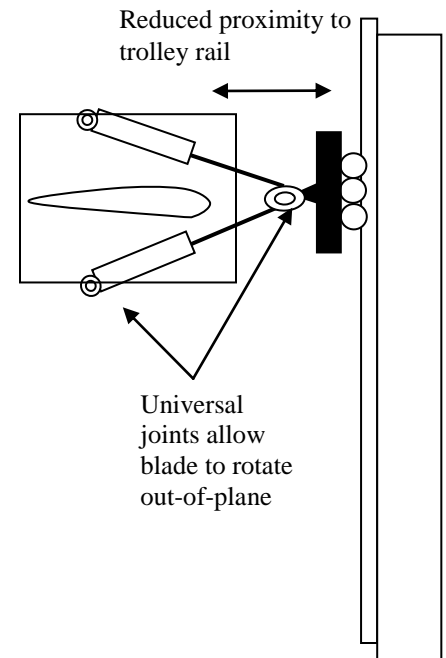


**Figure 3.4 Alternative embodiments of NREL's blade-mounted edgewise excitation system concepts**

As discussed, this design (embodiment 4) has many advantages over the other alternatives, so it is considered for more detailed analysis. Before proceeding to the dynamics and mechanics of the design, it is modeled in 3-D modeling software to work on the kinematics of the design. A very simple model is made in SolidWorks, as can be seen in Figure 3.5.

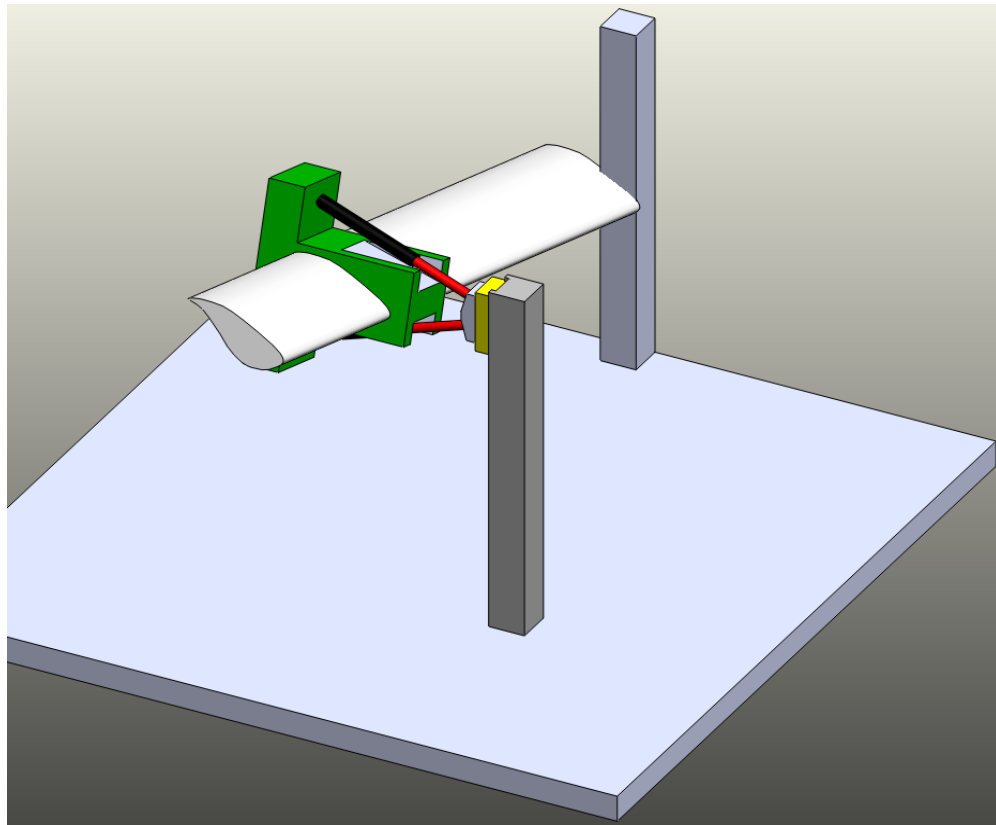


**Figure 3.5 Design of model in SolidWorks**

A closer view of the model showing different types of joints is shown below.

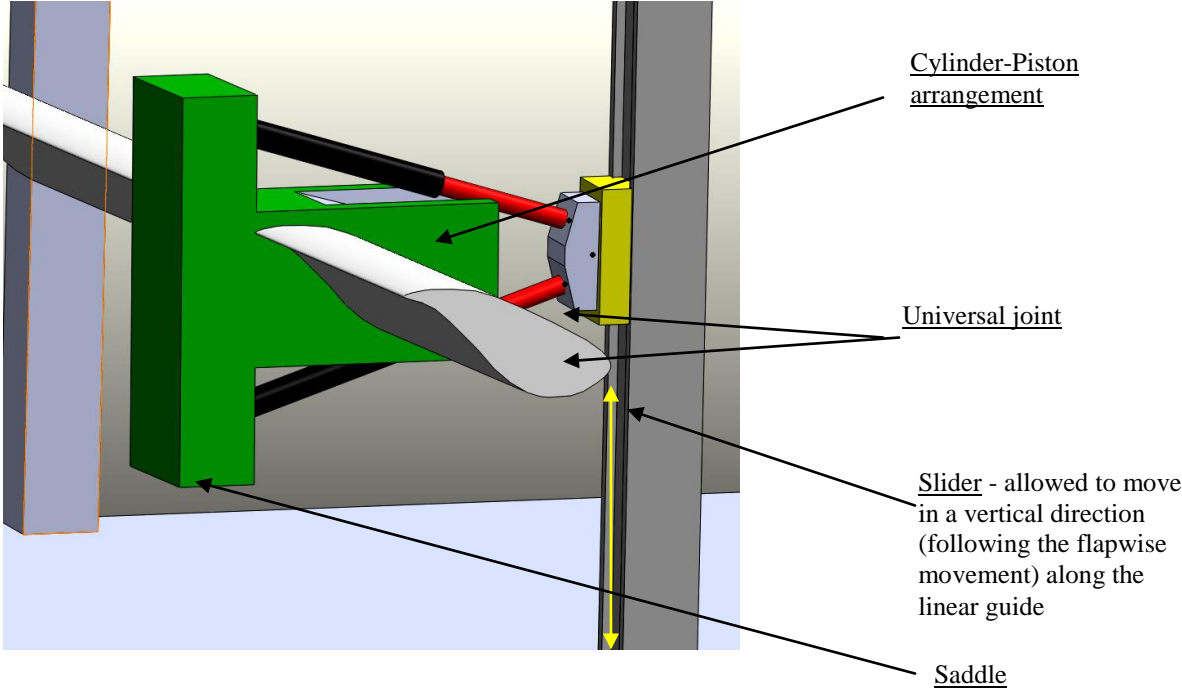


Figure 3.6 Model showing different types of joints

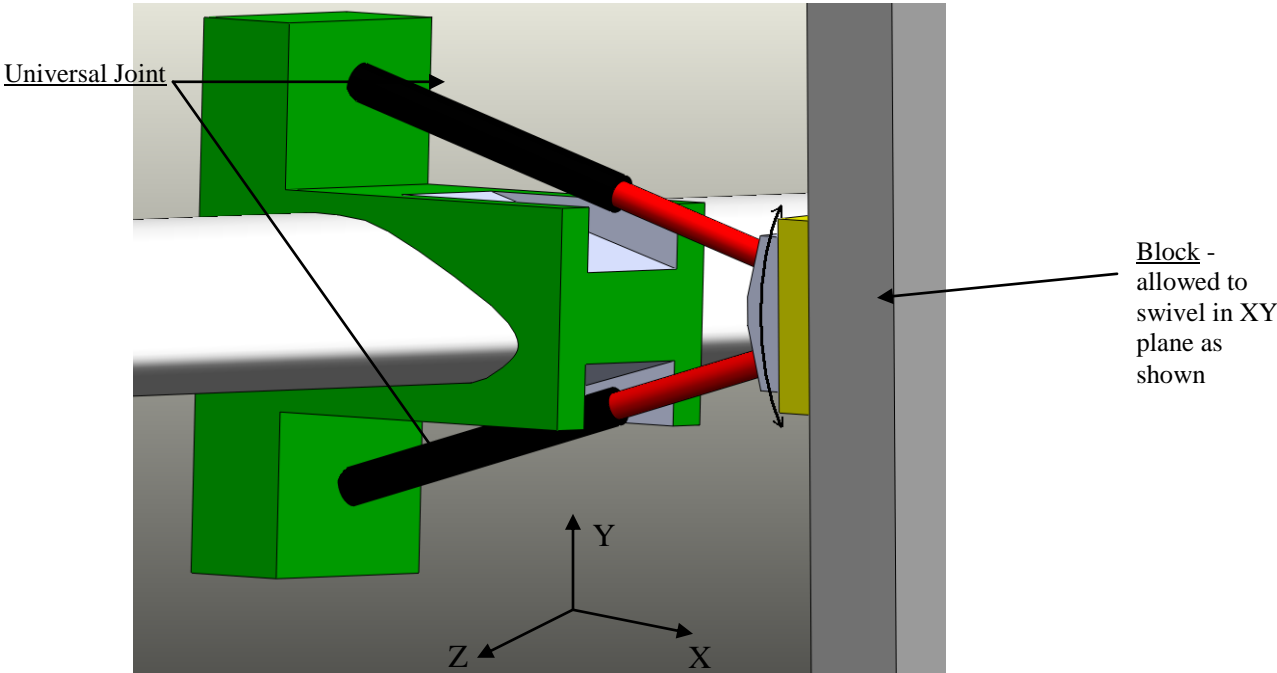
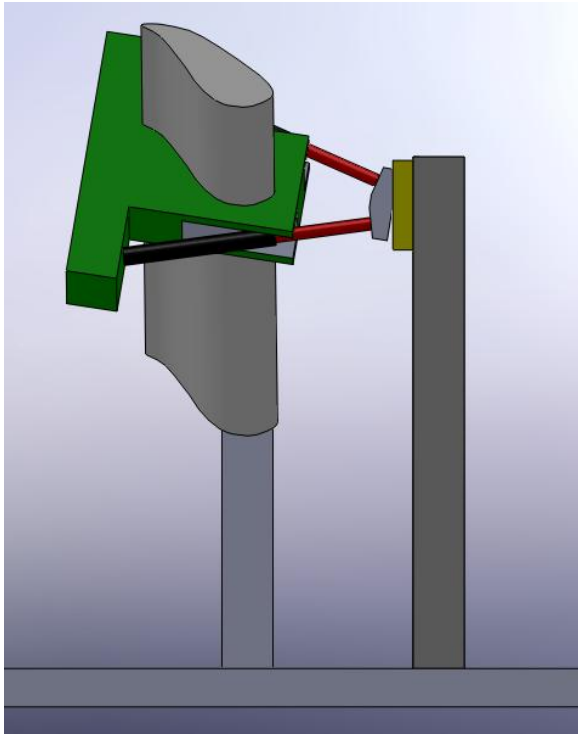
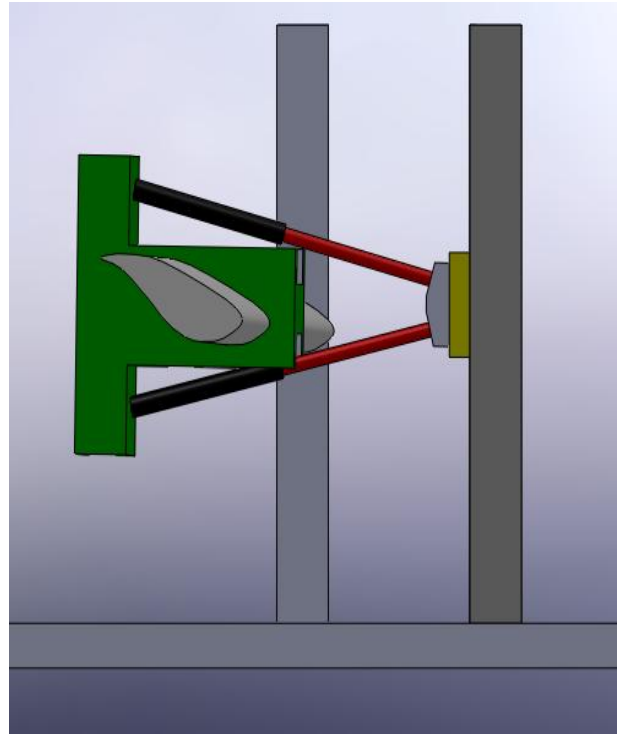


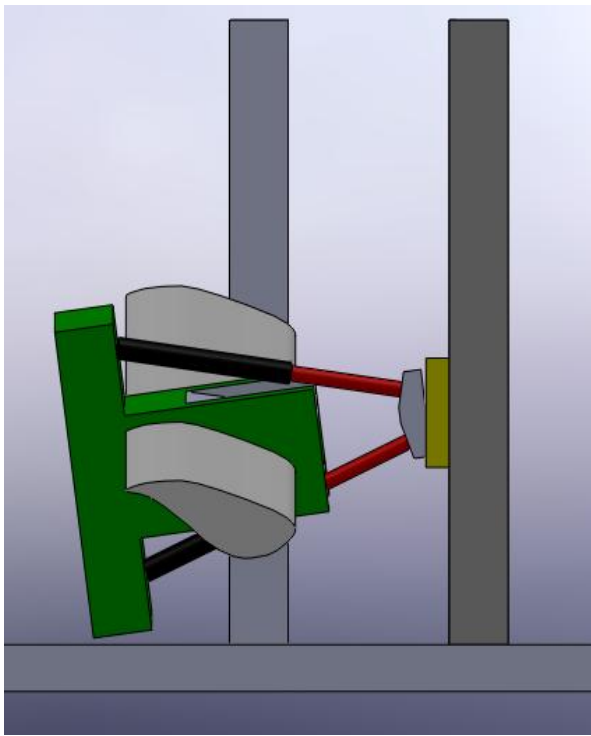
Figure 3.7 Closer view of the model



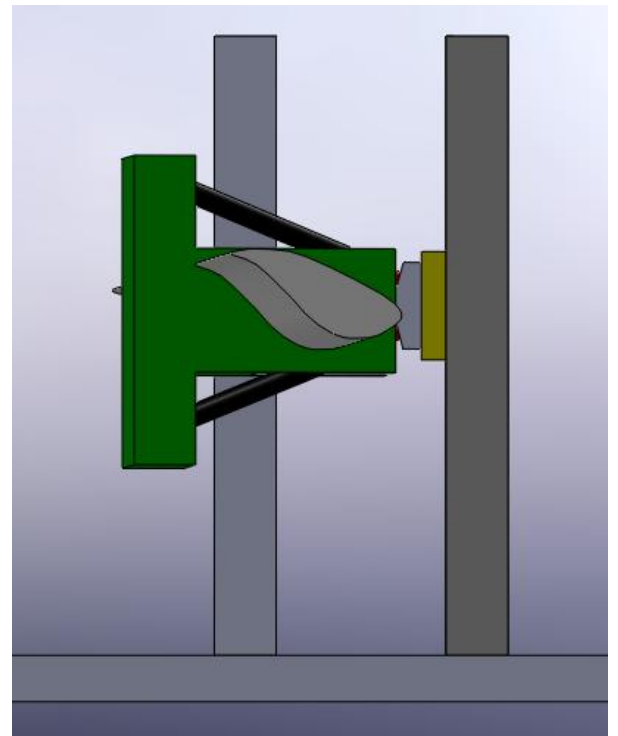
(a)



(b)



(c)



(d)

**Figure 3.8 Front View of the model at different positions during the test**

## **CHAPTER 4**

### **DESIGN REQUIREMENTS**

#### **4.1 Objective**

The whole design of the system is necessary to calculate the dynamics involved and the feasibility of the design. For further designing of this blade testing system, we need to know the various design requirements, viz., hydraulic requirements and linear guide rail system requirements. These calculations will help in estimating the cost of the whole test apparatus and can be a major deciding factor to use this system in near future.

#### **4.2 Method**

The design requirements and calculations are made taking a specific blade into consideration. The data for the blade was generated using software FAST for 5MW, 62m blade [18]. FAST which stands for Fatigue, Aerodynamics, Structure and Turbulence is an aeroelastic design code for horizontal axis wind turbines, was developed by Jason Jonkman at National Renewable Energy Laboratories (NREL).

In order to discuss testing of blades, it is important to recognize certain blade characteristics. The different blade properties are described in next section.

#### **4.3 Normalized blade Properties**

Although the blade properties depends a lot upon the manufacturer, the normalized distributions can be shown for reference, as it is very important to understand basic fundamental characteristics of blade. In this case, the blade data generated using FAST were interpolated according to the required normalized blade sections. The original



data and the interpolated data matched very closely and are shown in the following figures in this chapter.

### 4.3.1 Mass per unit length

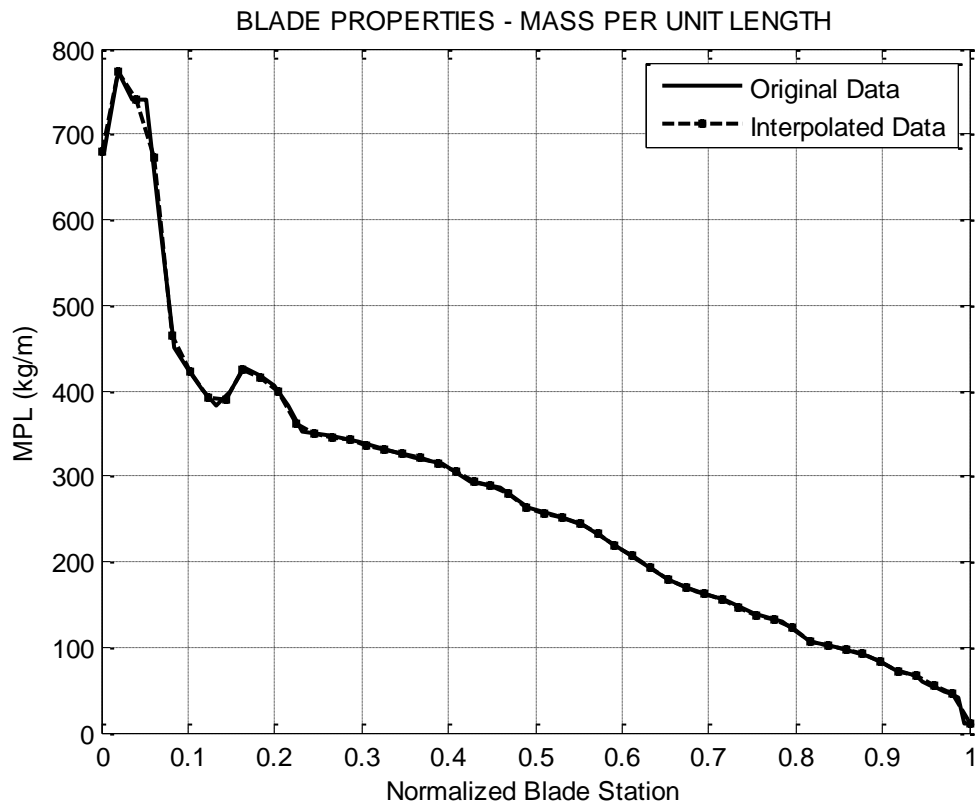


**Figure 4.1 Mass per unit length along normalized blade station**

In Figure 4.1, as we can see, mass per unit length drops significantly from 0 to 10%, because more material is needed at the root. This is required to secure the blade safely to the hub, which is further accomplished by bolting the blade at the root. Around 15-20% span of the blade, there is an increase in mass per unit length, which is due to maximum chord around this length. For the remaining 75-80% span of the blade, it has a linearly decreasing profile from max chord to the tip of the blade.

### 4.3.2 Chord Length

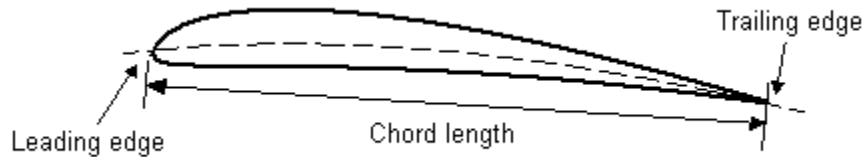


**Figure 4.2 Airfoil nomenclature showing chord length**

The straight line connecting the leading edge and trailing edge is the chord line of the airfoil, and the distance from the leading to the trailing edge measured along the chord line is designated as chord length as shown in Figure 4.2.

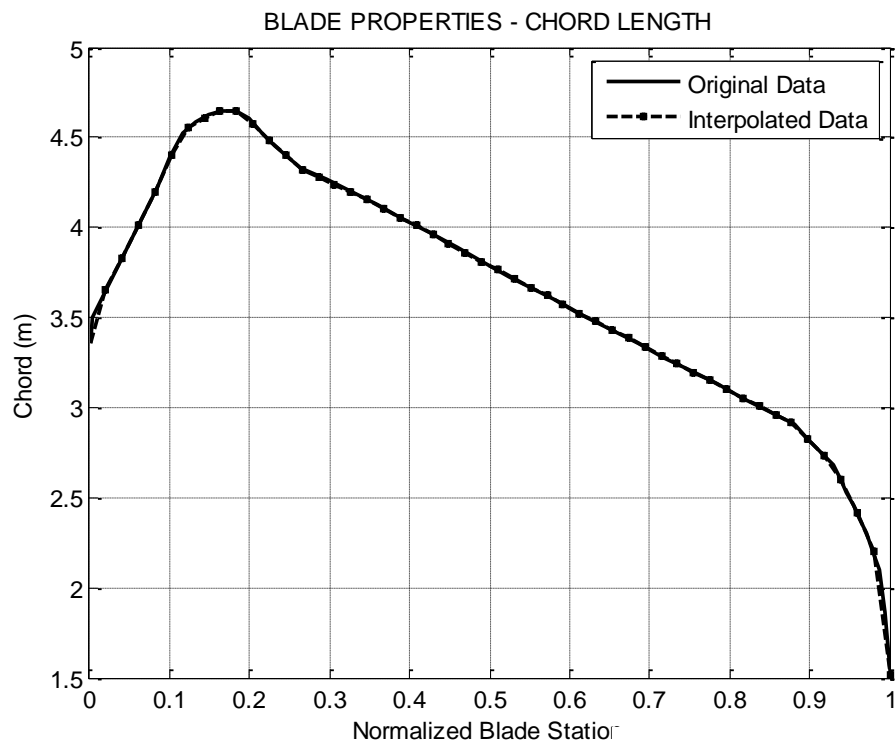


**Figure 4.3 Chord length along normalized blade station**

As shown in Figure 4.2, the maximum chord occurs at 15% station and is pretty much linear beyond this point to the tip of the blade. The chord length at root corresponds to the root circle diameter.

### 4.3.3 Flap Stiffness

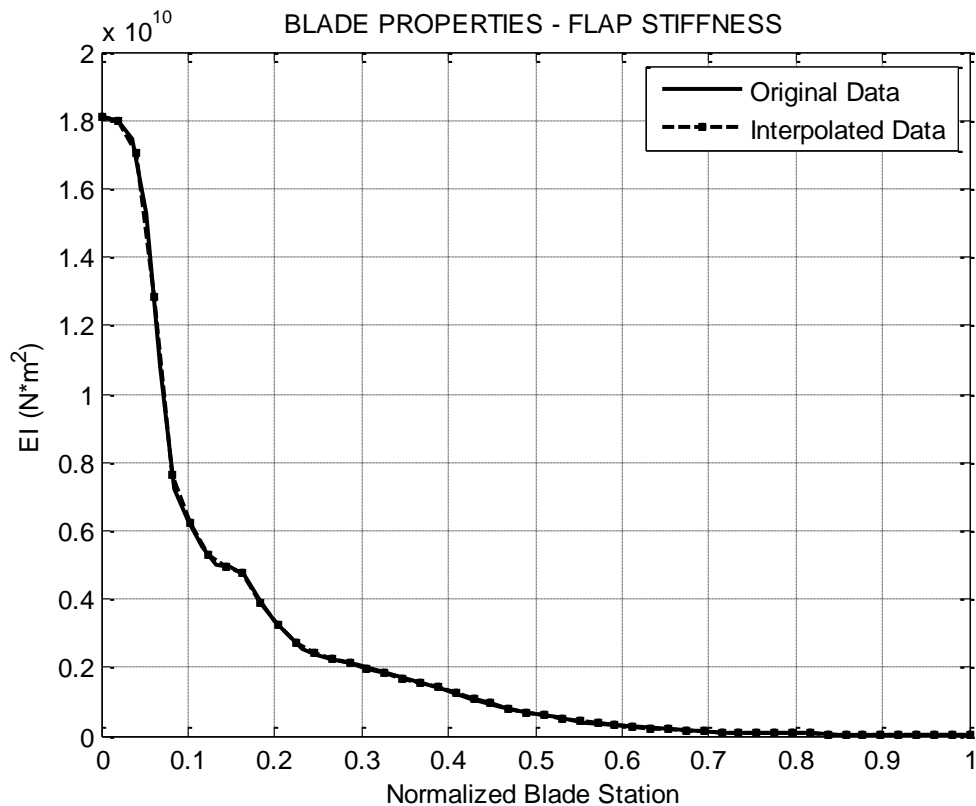


**Figure 4.4 Flap stiffness along the length of the blade**

The resistance to bending in the flapwise direction is referred to as flap stiffness of the blade. Flap stiffness as can be seen in the Figure 4.4, drops from the root to the point just before maximum chord location and then increases a little at maximum chord. This is again due to more material and resin at the root to accomplish safe securing of blade at the root. From the maximum chord to the tip of the blade, flap stiffness is not linear but is more or less shows an exponential decay. The flap stiffness depends largely on the locations of internal spars, thereby increasing the resistance to bending.

### 4.3.4 Edge Stiffness

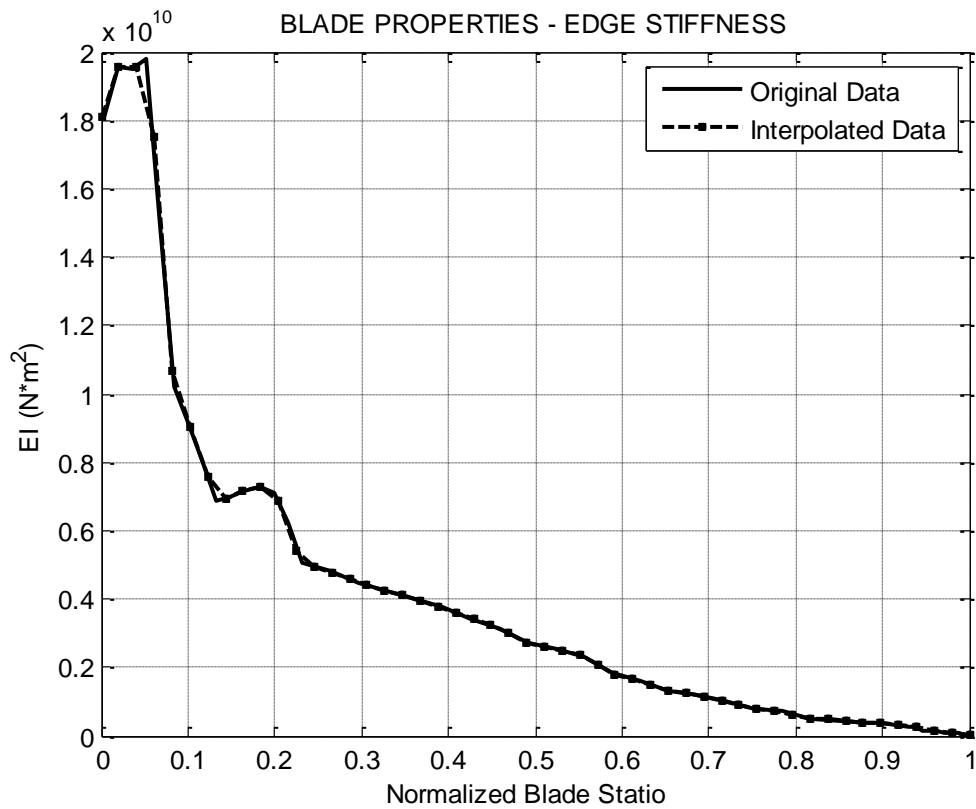


**Figure 4.5 Edge stiffness along the length of the blade**

The edge stiffness refers to the resistance to bending in the edgewise or lead lag direction. It has similar characteristics to the flap stiffness but the values are generally higher as can be observed from a shallower decay.

### 4.3.5 Axial Stiffness

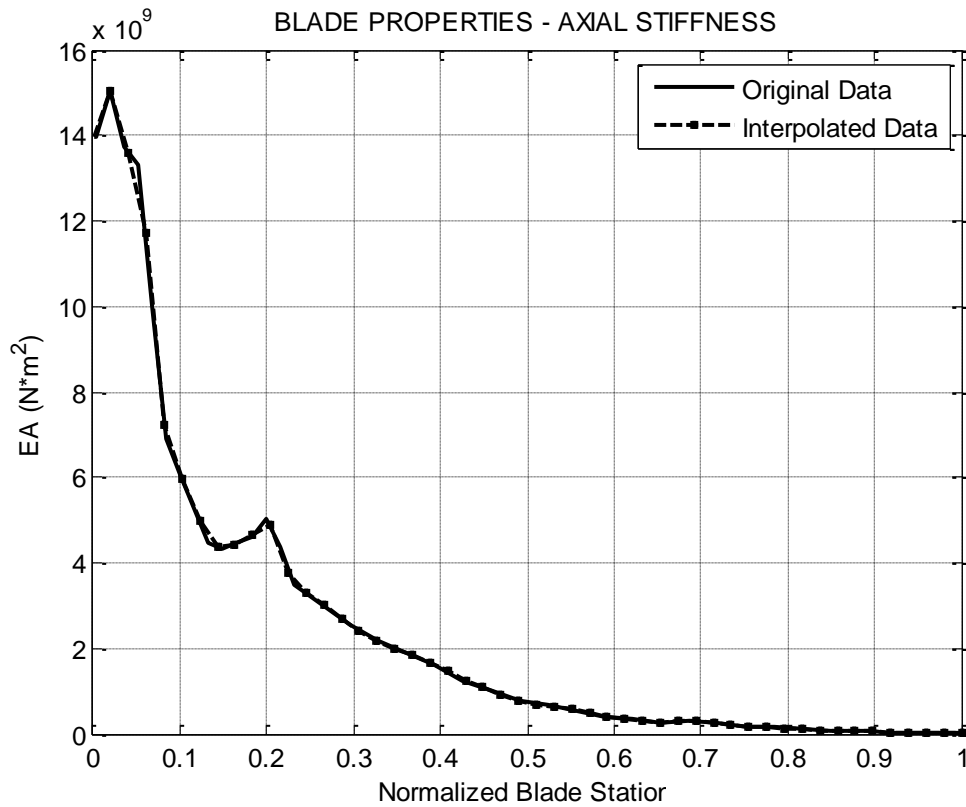


**Figure 4.6 Axial Stiffness along the length of the blade**

Resistance to elongation of the blade is referred to as axial stiffness. The value of axial stiffness depends upon the modulus of elasticity of the material used in constructing the blade and the amount of material in each cross-section. The value of modulus of elasticity may also change along the length of the blade due to different layups. Although axial stiffness is not large, so not so significant as compared to flapwise or edgewise stiffness, its value just has to be of the same order of magnitude or higher the flapwise stiffness.

### 4.3.6 Torsional stiffness

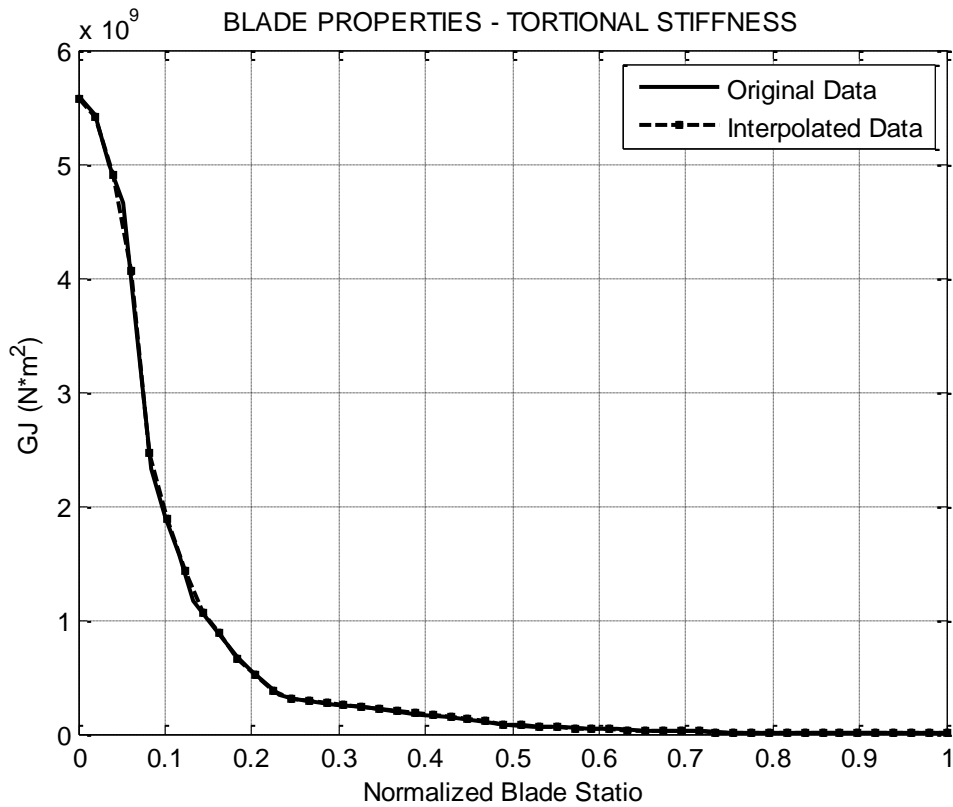


**Figure 4.7 Torsional stiffness along the length of the blade**

Torsional stiffness is the resistance to twisting of the blade between flapwise and edgewise directions. This resistance is highest at the root because of the geometry being circular. A quick drop in torsional stiffness facilitates twist coupling between the flapwise and edgewise directions. The trend in designing blade is to keep the torsional stiffness higher to reduce the twist so as to eliminate the deformation caused by applied torque on the blade.

## **4.4 Calculations & analysis**

The analysis of the blade, with and without saddles with the test configuration as discussed in chapter 3, Figure 3.4 (alternative embodiment 4) was done using a MATLAB code generated at NREL. Three different types of cases are considered:

1. Static case 1 – stationary blade without saddles, under its own weight
2. Static case 2 – stationary blade with saddles
3. Dynamic case – blade moving in the flapwise directions with saddles on it

### **4.4.1 About MATLAB Code**

The source code gets blade properties, target loads, and saddle specifications from an input excel file which then gets distributed into the finite element blade model and run through the appropriate test simulation. The blade properties are generated using software FAST for 5MW, 62m blade [18]. The source code features include the ability to generate missing properties and loads using curve fits based on blade length, as well as built in optimization routines to determine locations and loads of saddles. Once the target load has been determined, the applied load is calculated by combining the moments of several loading points to get a distributed load [21]

### **4.4.2 Static Analysis (blade without saddles, under its own weight)**

These calculations are based considering the blade in a stationary position mounted horizontally on a test stand without saddles, under its own weight. The static test code uses the finite element model to predict the loads and deflections of the blade during static testing. The target and applied loads can be specified using the input file or the code can predict the target load and then optimize the applied load to match. An

optimization routine (non-linear, trust-region-reflective algorithm based on the Newton method [22]) was employed to determine the saddle loads by minimizing the difference between the target load and the resulting applied load in a least squared sense. Once the applied loads are determined, the blade deflection is computed using a fourth order Runge-Kutta (RK4) numerical analysis method [23], which is defined by the equation

$$y_{n+1} = y_n + \frac{1}{6}h(2k_1 + 4k_2),$$

where  $y_n$  is the present value,  $h$  is the size of the interval,  $k_1$  corresponds to the slope of the element and  $k_2$  corresponds to the slope at the midpoint of the element. In this case, the interval is the element length and the slope is the applied load divided by the corresponding blade stiffness of the test direction.

The results and plots for this case, “static case 1” are summarized in table 4.1 and the following figures.

**Table 4.1 Static analysis (blade without saddles, under its own weight) calculations and results**

Blade weight	169.06 kN	38007 lbs
Blade mass	17234 kg	37994 lb
Centre of gravity location	20.586 m	67.54 ft
1st flap frequency	4.37 rad/s	0.70 Hz
2nd flap frequency	12.56 rad/s	2.00 Hz
3rd flap frequency	29.094 rad/s	4.63 Hz
1st edge frequency	6.99 rad/s	1.11 Hz
2nd edge frequency	25.84 rad/s	4.11 Hz
3rd edge frequency	59.56 rad/s	9.48 Hz
Tip deflection	1.02 m	3.34 ft
Root mean moment	3480 kN*m	2567 kip*ft



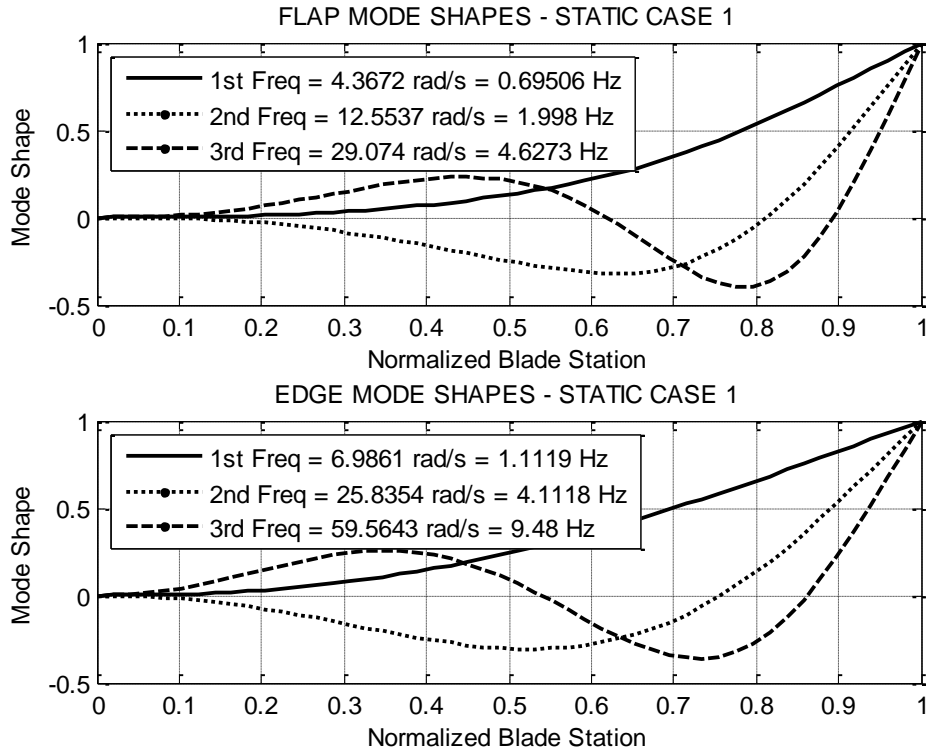


**Figure 4.8 Flap and edgewise mode shapes for static case (blade without saddles)**

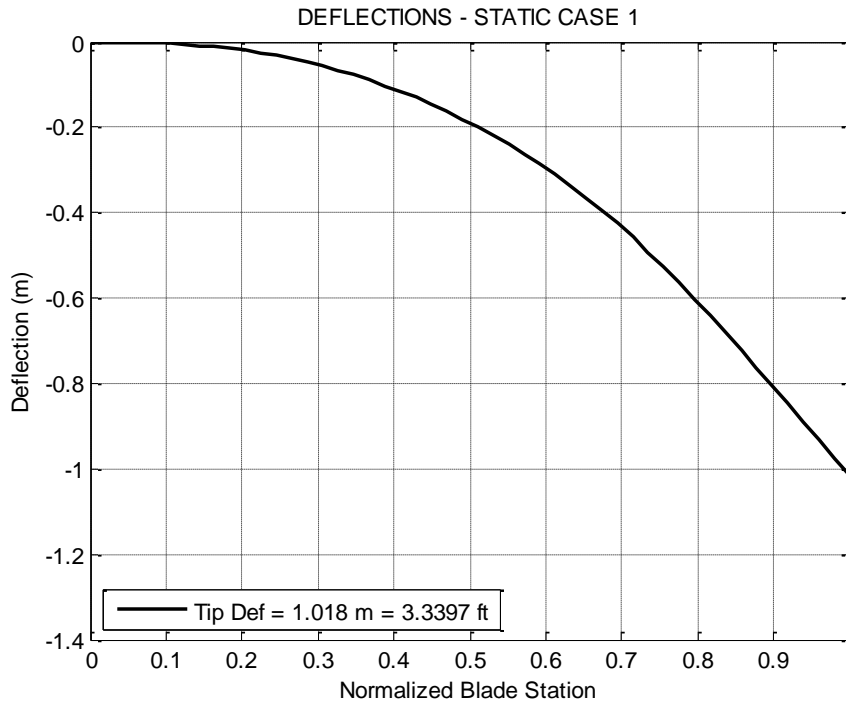


**Figure 4.9 Tip deflection when the blade is stationary (without saddles, under its own weight)**

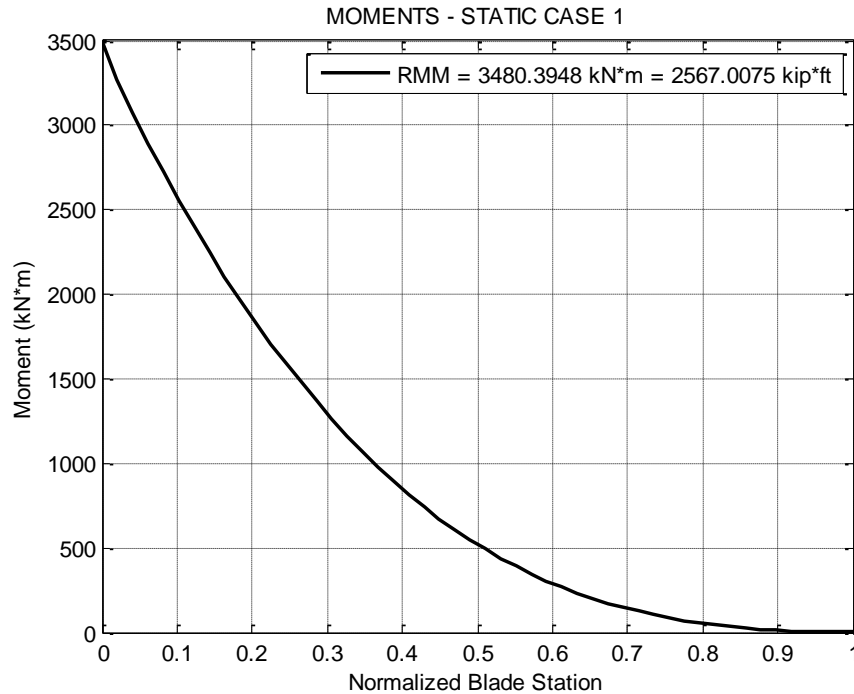


**Figure 4.10 Moment distribution along the length of the blade (without saddles, under its own weight)**

#### 4.4.3 Static & dynamic analysis (blade with saddles)

The fatigue test code uses the finite element model to predict the loads and deflections of the blade during fatigue testing. The target and applied loads can be specified using the input file or the code can predict the target load and then optimize the applied load to match. [21]

Historically, the target loads for fatigue testing are determined from S-N curves of material coupon tests (such as the MSU/DOE database for composite materials) and Goodman diagrams for one million cycles. This load is derived from parameters such as material composition, fiber orientation, resin compound, and manufacturing process, which are specific to each blade. In order to generate representative theoretical test loads in the absence of manufacturer supplied loads, curve fits were developed based on historical test loads observed at NREL in both the flapwise and edgewise directions. It

was assumed the orientation of the blade on the test stand (also referred to as clocking) is defined such that the flapwise direction is perpendicular to the ground and the edgewise direction is parallel to the ground. This results in some mean load in the flapwise direction due to the weight of the blade and test equipment as well as an alternating load, where as the edge loads are purely alternating loads. [21]

Once the target loads are determined, the applied load is computed from a dynamic moment analysis using the equation  $M_{ALT} = \sum m(\omega^2 y).x$  where  $m$  is the element mass,  $\omega$  is the system natural frequency,  $y$  is the blade deflection, and  $x$  is the moment arm. The applied load distribution can be tuned to match the either the target mean or alternating load distributions by adjusting the saddle weights which modifies the mode shapes. The same optimization routine employed previously [22] was modified to find the required saddle weights. The alternating load is combined with the mean load to obtain the operating loads in the flapwise direction [21]

To perform fatigue testing of the blades, the blade is subjected to forces at different sections so as to match the required moment distribution along the length of the blade. This section describes the analysis done having two saddles at different blade locations, in addition to the saddle at 70% location. Various combinations were used for this analysis so as to optimize the saddle weight and moment distribution along the blade length. The most appropriate combination was found to have two saddles at 50% and 85% of the blade length. Results for static and dynamic analysis of the blade having two saddles at 50% and 85%, and one at 70% of the blade length are summarized in table 4.2. Saddle 1, 2 and 3 corresponds to blade station 50%, 70% and 85% respectively. Static analysis shows the calculations when the blade is not in motion and is sitting on the test

stand with saddles mounted on it, while dynamic analysis assumes the blade moving in flapwise direction, with saddles mounted over it. These cases are labeled as “static case 2” and “dynamic case” respectively. RMS fit is referred to as root mean square deviation which is a measure of the difference between the values of the target load and applied load.

#### **4.4.3.1 Static analysis**

**Table 4.2 Static analysis (blade with saddles) calculations and results**

Weight of Saddle 1	13519 N	3039 lbs
Weight of Saddle 2	10909 N	2452 lbs
Weight of Saddle 3	44549 N	10015 lbs
Blade Weight	238 kN	53514 lbs
Blade Mass	24265 Kg	53495 lb
Centre of gravity location	28.3 m	93 ft
1st flap frequency	0.365 Hz	2.3 rad/sec
1st edge frequency	0.62 Hz	3.9 rad/sec
Tip Deflection	3.1 m	10 ft
Root mean moment	6736 kN.m	4968 kip.ft

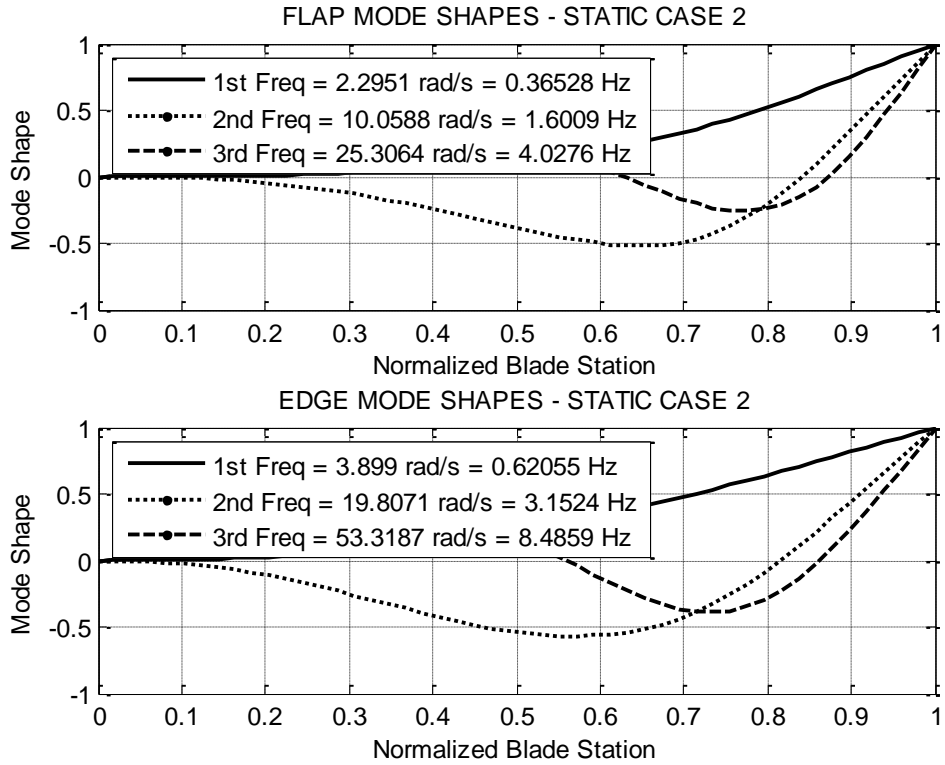


**Figure 4.11 Flap and edgewise mode shapes for static case 2 (blade with saddles)**

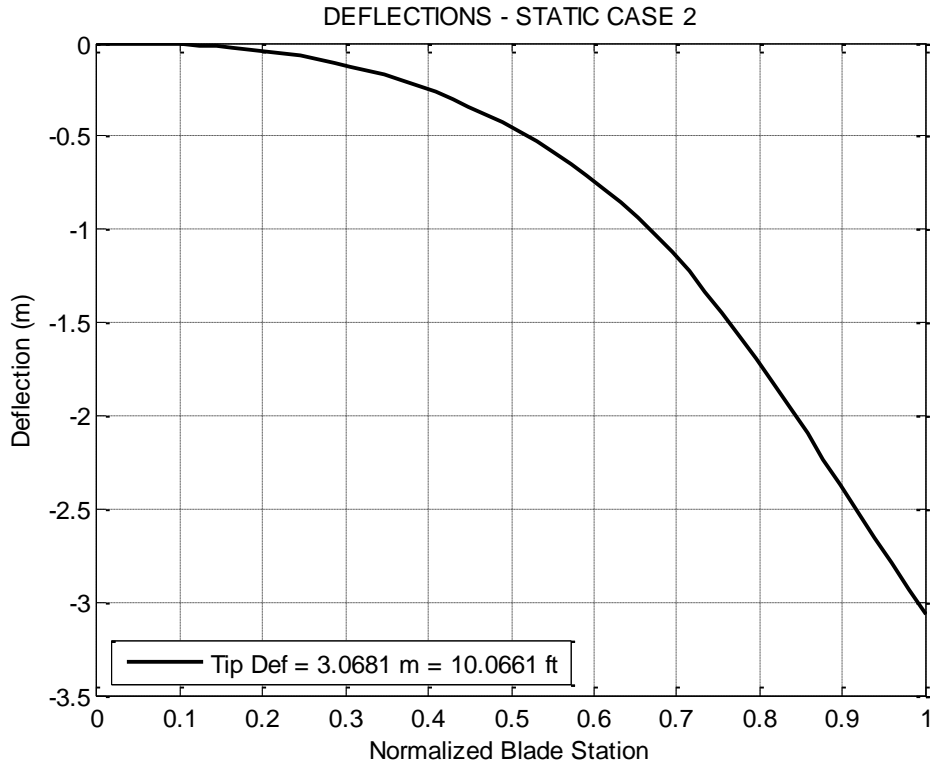


**Figure 4.12 Tip deflection when the blade is stationary (with saddles on)**

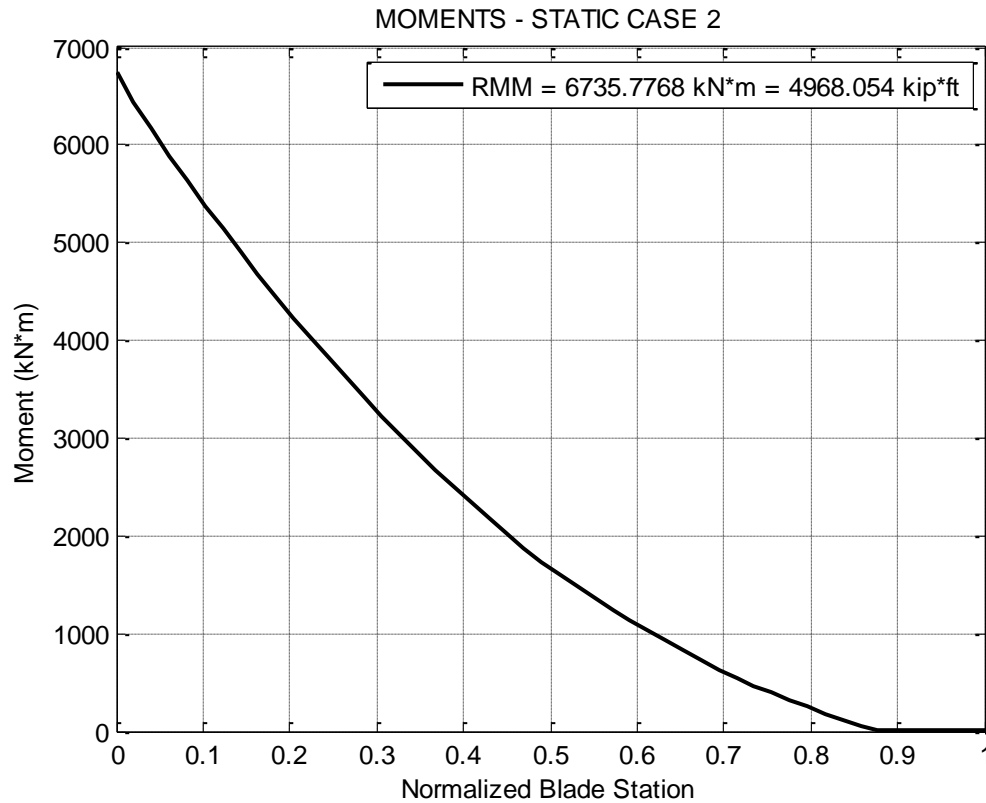


**Figure 4.13 Moment distribution along the length of the blade (with saddles)**

#### **4.4.3.2 Dynamic analysis**

Dynamic analysis is done with saddles attached to the blade at three different position so as to match the bending moment distribution along the length of the blade. Test configuration is as shown in Figure 3.4 (alternative embodiment 4). Blade resonant excitation system (BREX) is used for flapping the blade at the resonant frequency in the flapwise direction and inclined actuators impart the desired force in the edgewise direction.

**Table 4.3 Dynamic analysis calculations and results**

Flap Tip Deflection	4.36 m	14.30 ft
Flap Root Alt Moment	5973.43 kN.m	4405.78 kip.ft
Edge Tip Deflection	1.70 m	5.57 ft
Edge Bending root Moment	10469.44 kN.m	7721.87 kip.ft

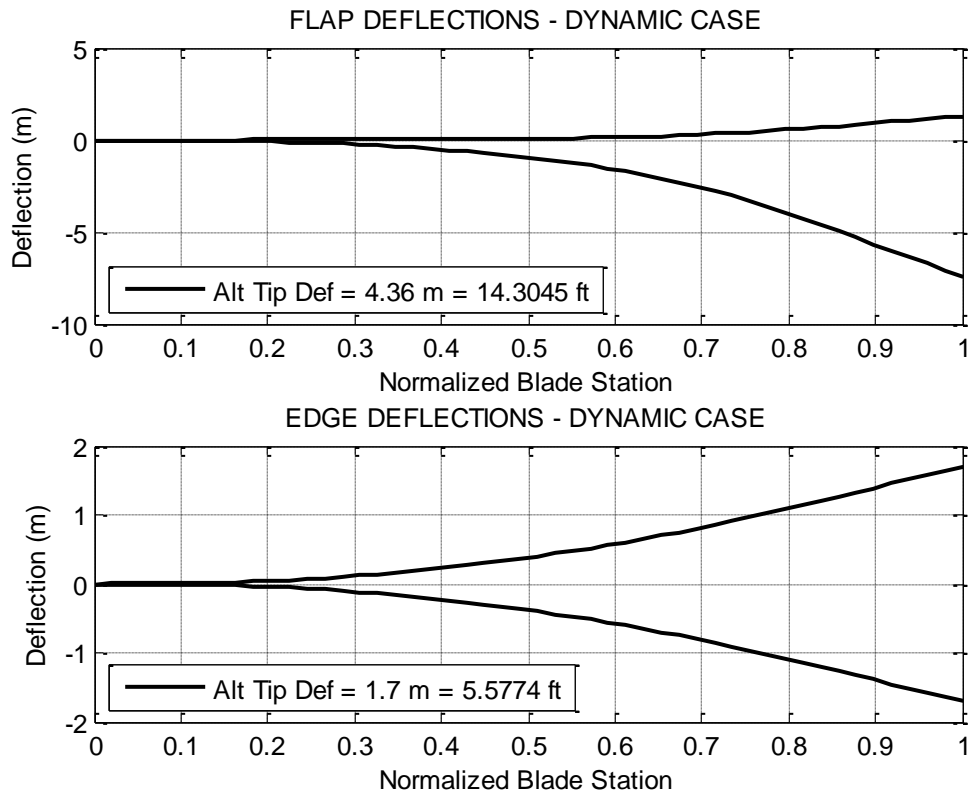


**Figure 4.14 Flap and edge deflections along the length of the blade for dynamic case**

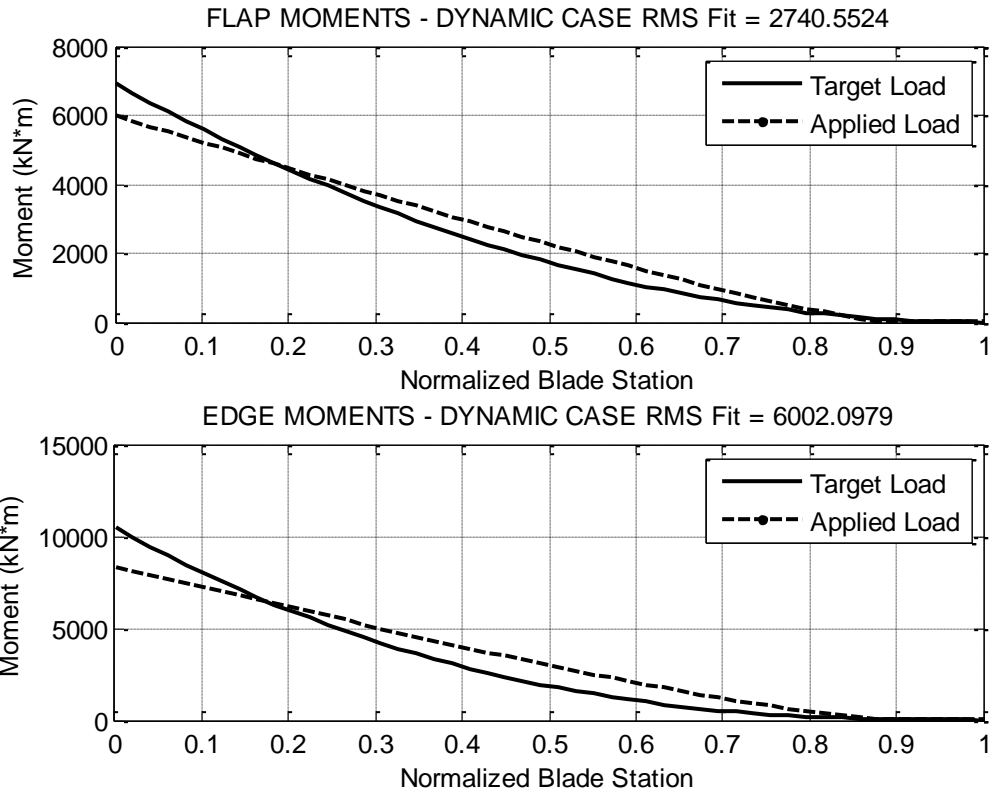


**Figure 4.15 Flap and edge moments along the length of the blade for dynamic case**

**4.5 Hydraulic requirements**

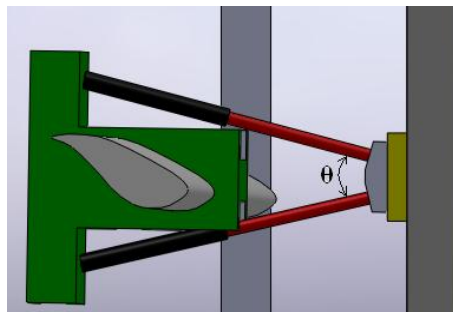


**Figure 4.16 Angle between the actuators**

The very first thing we need to know is the hydraulic force required to be delivered by one actuator. The normal operating pressure for the hydraulic cylinders used for blade testing is 3000 psi. The angle between the inclined actuators is  $\theta$ , as shown in Figure 4.16



If the guide rail assembly is allowed to move on its own, the B-rex system has to apply much greater force taking the weight of the hydraulic actuators, universal joints and guide rails assembly into consideration. This is resolved by attaching another hydraulic actuator which moves the guide rail assembly up and down simultaneously with the flapwise motion of the blade, taking the weight of hydraulic actuators and linear guide rail assembly.

Now, edge root bending moment at 70% blade station = 10469 kNm

$$\begin{aligned} \text{So, the total force required} &= \frac{\text{Edge root bending moment}}{\text{Length of the blade at 70\% station}} \\ &= \frac{10469}{0.7 * 61.33} = 243.87 \text{ kN} \end{aligned}$$

As this force is being delivered by two actuators inclined at an angle  $\theta$ , the force

$$\text{delivered by one actuator} = \frac{\text{Total force required}}{2 * \cos\theta}$$

$$\text{Stroke length required for an actuator} = \frac{2 * \text{Deflection at half amplitude}}{\cos\theta}$$

$$\text{Using the equation, Pressure} = \frac{\text{Force}}{\text{Area}},$$

we have, Pressure = 3000 psi,

$$\Rightarrow \text{Pressure} = \frac{\text{Force}}{\frac{\pi}{4} d^2}$$

$$\text{So the cylinder diameter, } d = 2 * \sqrt{\frac{\text{Force}}{\text{Pressure} * \pi}}$$

Based on above equations, the specifications for the hydraulic cylinder are summarized in table 4.4.

**Table 4.4 Hydraulic system requirements**

Angle between actuators (degrees)	30	40
Force to be delivered by one actuator (kN)	126 (28.38 kip)	130 (29.17 kip)
Edge frequency (Hz)	0.62	0.62
Edge Deflection half amplitude at 70% (m)	0.8	0.8
Stroke length required (m)	1.65	1.7
Cylinder diameter (in)	3.47	3.52
Flow rate (gpm)	192	197

Based on the above requirements, a company named MTS who manufacture hydraulic cylinders worked with me to define the hydraulic cylinder requirements and setting up a price quote for the product.

A system configured for this application would require actuators, hydraulic power units (HPU), control system, hydraulic distribution, fixturing and engineering support. A rough estimate might look like something like this:

- Qty. 2, 35 kip, 70in stroke actuators, 400 gpm servo valves - \$ 250k
- Qty. 3, 180 gpm HPU's - \$ 550k
- Multi-channel control system- \$ 150k
- Hydraulic distribution (depends on lab layout) - \$ 100k
- Custom designed test fixturing - \$ 200k
- Installation support \$ 25k

A system like this would cost roughly around \$1.2 million. The product specification as provided by MTS can be found below.

#### **4.6 MTS Series 201 Hydraulic Actuator**

This section includes the literature about the product as provided by MTS. MTS Series 201 hydraulic actuators are heavy duty, fatigue rated force generators designed for long stroke and/or low dynamic applications. Compatible with MTS' feedback and

control components, these actuators provide precise performance ideal for low frequency test and simulation applications. It is flexible enough to meet force and motion control needs. These actuators are available in 11 force ratings, 4 standard lengths and make to order custom lengths.

MTS 201 Actuators are designed for superior responsiveness and reliability. The actuator design incorporates high and low pressure seals and a drain arrangement. These features provide lower friction and control oil leaks. Nonmetallic bearings provide side load tolerance and greater resistance to galling thereby extending operational life.



**Figure 4.17 MTS Series 201 Hydraulic Actuator**

#### **4.6.1 Benefits**

##### *Large Selection*

Available in tension force ratings from 7 to 400 kip with proportionally higher compressive force ratings

##### *Non Metallic Bearing*

High quality non-metallic bearings provide long life and resist galling failures.

##### *Precise Control*

Designed for use with MTS' closed looped servo-hydraulic accessories.

### *Ease of Service*

A special housing design permits piston rod bearings and seals to be replaced without dismantling the cylinder/end cap assembly.

### *Range of Application*

Targeted for low frequency applications that requires accurate servo-controlled performance.

### *Economical Design*

Closed-loop servo-hydraulic actuator features in a streamlined design.

## **4.6.2 Options**

### *Force Rating*

With a wide variety to select from, series 201 Actuator can be matched to our application for the best performance and spatial fit. Tension force ratings to 400 kip and compressive to 580 Kip

### *Stroke Length*

201 Actuators are available in standard stroke lengths of 10, 20, 30, and 40 inches and in custom stroke lengths providing the flexibility to meet a wide variety of requirements.

### *Transducers*

High quality MTS transducers are available for the 201 Actuator series. These actuators are compatible with MTS load cells, LVDTs, and magnetostrictive transducers.

### *Mountings*

A variety of mounting methods are available including pedestal, clevis, and swivel designs. For applications with load transitions that cross from tension to compression, MTS' 249 Swivel with anti-backlash adjustment is the perfect solution.

### *Servovalve*

The MTS 252 Servovalve, rated from 1 to 16.5 gpm, mounts directly to the actuator. If more flow is required, a manifold for adding a second servovalve is a standard option. When greater flows are required, custom actuators are available. In our case, the servo valves has to be custom designed to have a flow rate of 400gpm.

### *Life Kit*

Provides secure balanced life equipment for handling actuators.

### 4.6.3 Specifications

#### 201 Series Actuator Force Rating, Piston Area

Model	Piston Area				Force			
	Tension Area		Compression Area		Tension		Compression	
	in <sup>2</sup>	cm <sup>2</sup>	in <sup>2</sup>	cm <sup>2</sup>	kip	kN	kip	kN
201.17	2.5	16.2	4.9	31.7	7	32	14	63
201.20	5.2	33.3	8.3	53.5	15	66	24	107
201.25	7.7	49.4	12.6	81.1	22	99	36	162
201.30	12.6	81.1	19.6	126.7	36	162	57	253
201.35	18.7	120.3	28.3	182.4	55	240	80	365
201.40	22.6	145.7	38.5	248.3	65	290	110	495
201.45	34.4	221.7	50.3	324.3	100	445	145	650
201.60	50.3	324.3	78.5	506.7	145	650	230	1015
201.70	74.6	481.4	113.1	729.7	215	965	330	1460
201.80	103.7	668.9	153.9	993.2	300	1340	445	1985
201.90	137.4	886.7	201.1	1297.2	400	1775	590	2595

#### 201 Series Basic Cylinder Dimensions

Model	Rod Dia.		A		B		C		D		E		F		G	
	in	mm	in	mm	in	mm	in	mm	US cust.	SI metric	in	mm	in	mm	in	mm
201.17	1.75	44.5	4.9	124	7.9	199.9	2.1	53.8	1"-14	M27 x 2	1.8	44.5	2.00	50.8	2.0	51
201.20	2.0	50.8	5.1	129	8.4	212.6	2.1	53.8	1"-14	M27 x 2	1.8	44.5	2.00	50.8	2.0	51
201.25	2.5	63.5	5.1	129	8.4	212.6	2.1	53.8	1"-14	M27 x 2	1.8	44.5	2.00	50.8	2.0	51
201.30	3.0	76.2	5.6	141	9.3	235.5	2.6	66.5	1 1/2"-12	M36 x 2	2.3	57.2	2.00	50.8	2.0	51
201.35	3.5	88.9	5.8	148	10.0	254.8	2.9	73.2	1 1/2"-12	M36 x 2	2.3	57.2	2.00	50.8	2.0	51
201.40	4.5	114.3	7.3	185	11.0	279.4	3.8	95.3	2"-12	M52 x 2	2.3	57.2	2.00	50.8	2.3	57
201.45	4.5	114.3	7.3	185	11.9	302.3	3.8	95.3	2"-12	M52 x 2	2.3	57.2	2.00	50.8	2.3	57
201.60	6.0	152.4	9.08	231	13.65	346.7	5.0	127.0	3"-12	M76 x 2	3.0	76.2	2.0	50.8	2.5	64
201.70	7.0	177.8	10.2	259	16.0	405.6	5.6	142.7	3 1/2"-12	M90 x 2	3.5	88.9	2.00	50.8	2.8	70
201.80	8.0	203.2	10.5	265	16.9	429.3	5.6	142.7	3 1/2"-12	M90 x 2	3.5	88.9	2.00	50.8	2.8	70
201.90	9.0	228.6	11.0	278	18.4	467.9	5.6	142.7	4 1/2"-8	M125 x 4	4.5	114.3	2.00	50.8	2.8	70

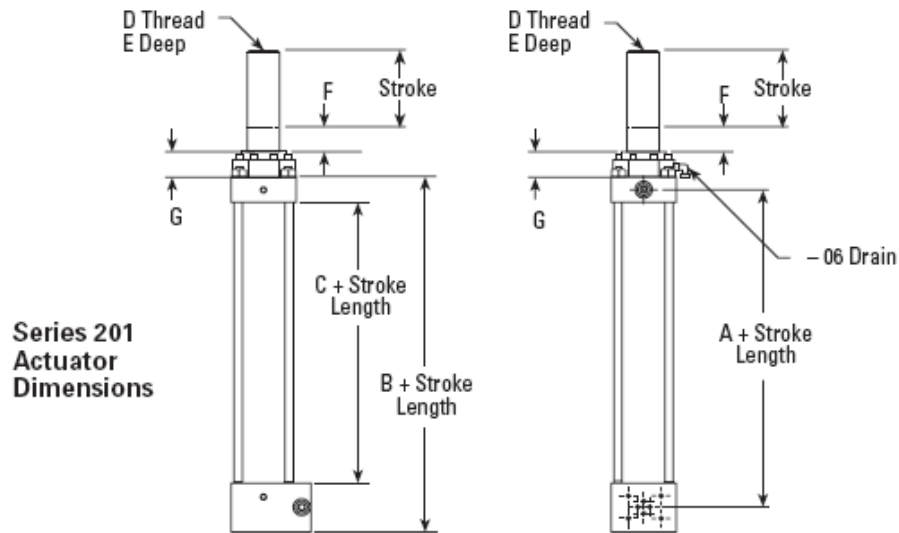


Figure 4.18 Actuator Specification drawing

#### **4.6.3.1 Rod diameter**

The piston rod is subjected to a load of 130 kN (~30kips). Looking at the chart for 201 series actuator force rating, it was found that series 201.30 hydraulic cylinders has to be used here. Looking at the specification chart, we have rod diameter of 3.0 inches (76.2mm) for series 201.30

#### **4.6.3.2 Inner & Outer diameter of cylinder**

Inner diameter of cylinder,  $d_i = 3.47 \text{ in} = 88.13 \text{ mm}$

To calculate outer diameter of the cylinder, we can use the equation

$$\sigma = P \cdot \frac{r}{t} = P \cdot \frac{d_i/2}{(d_o - d_i)/2}$$

Where,  $t$  = thickness of the cylinder,

$d_o$  = outer diameter of the cylinder,

$d_i$  = inner diameter of the cylinder.

Also, incorporating a factor of safety (FOS) of 2.5,

$$\text{We get, } \sigma_{cylinder} = P \cdot \frac{d_i}{d_o - d_i} \times FOS$$

Assuming the material of the cylinder and tie rods to be mild steel, for which

$\sigma = 410\text{MPa} = 60,000 \text{ psi}$ , the equation above gives,

$$d_o = 99.14 \text{ mm}$$

$$\text{Hence, wall thickness, } t = \frac{d_o - d_i}{2} = (99.14 - 88.13) / 2 = 5.5\text{mm}$$

Now selecting the standard size for tubes, we have outer diameter of 101.6 mm (4 inches) with wall thickness of 6.353 mm (0.25 inches). [19]

So summarizing all, we have

Outer diameter of cylinder = 101.6 mm

Wall thickness = 6.353 mm

Inner diameter of cylinder = 88.9 mm

#### 4.7 Flange specifications

At the end of the cylinder, a flange has to be attached which act as a mounting. We have outer diameter of cylinder of 101.6 mm. The available flanges in the market were looked up and a catalog brochure of a company named Walter Stauffenberg GmbH & Co. KG was found to serve the purpose. For this application, the SAE single part butt weld flange can be used with the product description BFX-309-ST-103/89. The drawing and specifications for the flange are given below in Figure 4.19 and table 4.5

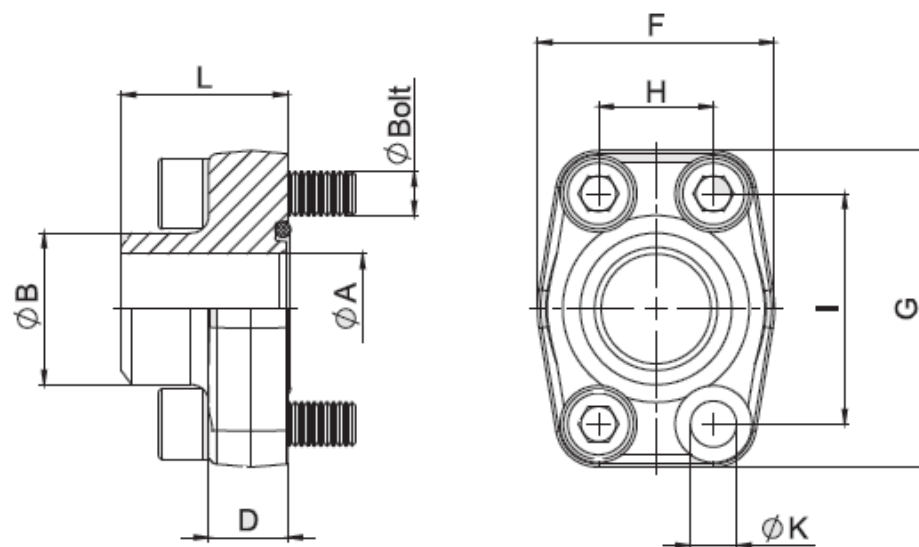


**Figure 4.19 Drawing of SAE single part butt weld flange**

**Table 4.5 Specifications of SAE single part butt weld flange**

Max. Betriebsdruck [bar] ** Max. Working Pressure [bar] **		Nenngröße Nominal Size		Artikelbezeichnung Article Description	Abmessungen [mm] Dimensions [mm]									für Schrauben for Bolts			
Schrauben 8.8 Bolts 8.8	Schrauben 10.9 Bolts 10.9 (MH)	ISO [DN]	SAE [inch]	SAE-Anschweißflansch SAE Single-Part Butt Weld Flange	ØA	ØB	D	F	G	H	I	L	ØK**	metr.**3	UNC		
<b>Standarddruck-Baureihe (nach ISO 6162-1)</b>																<b>3.000-PSI-Baureihe</b>	
Standard Pressure Series (according to ISO 6162-1)																3.000 PSI Series	
350	350	13	1/2"	BFX-301-ST-21,6/13	13	21,6	16	47	57	17,5	38,1	36	8,7	M8x30	5/16"-18x1"1/4		
350	350	13	1/2"	BFX-301-ST-17,5/13	13	17,5	16	47	57	17,5	38,1	36	8,7	M8x30	5/16"-18x1"1/4		
350	350	19	3/4"	BFX-302-ST-27,2/19	19	27,2	18	50	67	22,3	47,6	36	10,5	M10x35	3/8"-16x1"1/4		
250	315	25	1"	BFX-303-ST-34/25	25	34	18	54	72	26,2	52,4	38	10,5	M10x35	3/8"-16x1"1/4		
200	250	32	1"1/4	BFX-304-ST-42,8/32	32	42,8	21	68	82	30,2	58,7	41	11,7 (12,5)	M10x40 (M12x40)	7/16"-14x1"1/2		
200	200	38	1"1/2	BFX-305-ST-48,6/38	38	48,6	25	79	96	35,7	69,8	44	13,5 (14,5)	M12x45 (M14x45)	1/2"-13x1"1/2		
160	200	51	2"	BFX-306-ST-61/51	51	61	25,5	88	102	42,9	77,8	45	13,5 (14,5)	M12x45 (M14x45)	1/2"-13x1"1/2		
100	160	64	2"1/2	BFX-307-ST-76,6/63	63	76,6	26	101	115	50,8	88,9	50	13,5 (14,5)	M12x45 (M14x45)	1/2"-13x1"3/4		
100	160	76	3"	BFX-308-ST-92/73	73	92	27,5	127	137	61,9	106,4	50	17	M16x50	5/8"-11x1"3/4		
35	35	89	3"1/2	BFX-309-ST-103/89	89	103	27,5	138	155	69,9	120,7	50	17	M16x50	5/8"-11x2"		
35	35	102	4"	BFX-310-ST-115,5/99	99	115,5	27,5	147	163	77,8	130,2	50	17	M16x50	5/8"-11x2"		
35	35	127	5"	BFX-311-ST-140,2/120	120	140,2	28	180	184	92	152,4	50	17	M16x55	5/8"-11x2"1/4		

Looking at the nominal size of the flange used, SAE single part blind flange was selected with nominal size of 3½ inch having product name BFX-309-CP which has the specifications as summarized below:

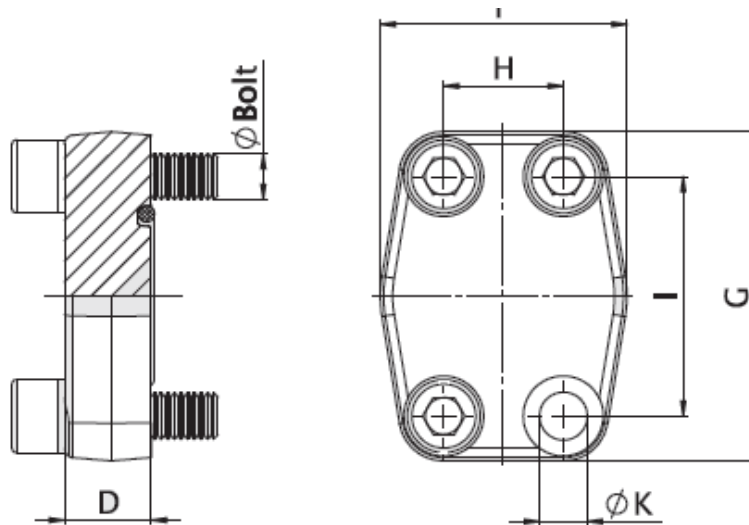


**Figure 4.20 Drawing of SAE single part blind flange**



**Table 4.6 Specifications of SAE single part blind flange**

Max. Betriebsdruck [bar] **1 Max. Working Pressure [bar] **1		Nenngröße Nominal Size		Artikelbezeichnung Article Description	Abmessungen [mm] Dimensions [mm]						für Schrauben for Bolts		
Schrauben 8.8 Bolts 8.8	Schrauben 10.9 Bolts 10.9 (MH)	ISO [DN]	SAE [inch]	SAE-Verschlussflansch SAE Single-Part Blind Flange	D	F	G	H	I	ØK**3	metr. **3	UNC	
<b>Standarddruck-Baureihe (nach ISO 6162-1)</b> Standard Pressure Series (according to ISO 6162-1)												<b>3.000-PSI-Baureihe</b> 3.000 PSI Series	
350	350	13	1/2"	BFX-301-CP	16	47	57	17,5	38,1	8,7	M8x30	5/16"-18x1"1/4	
350	350	19	3/4"	BFX-302-CP	18	50	67	22,3	47,6	10,5	M10x35	3/8"-16x1"1/4	
250	315	25	1"	BFX-303-CP	19	54	72	26,2	52,4	10,5	M10x35	3/8"-16x1"1/4	
200	250	32	1"1/4	BFX-304-CP	18	68	82	30,2	58,7	11,7 (12,5)	M10x40 (M12x40)	7/16"-14x1"1/2	
200	200	38	1"1/2	BFX-305-CP	20	79	96	35,7	69,9	13,5 (14,5)	M12x45 (M14x45)	1/2"-13"x1"1/2	
160	200	51	2"	BFX-306-CP	20	88	102	42,9	77,8	13,5 (14,5)	M12x45 (M14x45)	1/2"-13"x1"1/2	
100	160	64	2"1/2	BFX-307-CP	20	101	115	50,8	88,9	13,5 (14,5)	M12x45 (M14x45)	1/2"-13"x1"3/4	
100	160	76	3"	BFX-308-CP	24	127	137	61,9	106,4	17	M16x50	5/8"-11x1"3/4	
35	35	89	3"1/2	BFX-309-CP	22	138	155	69,8	120,7	17	M16x50	5/8"-11x2"	
35	35	102	4"	BFX-310-CP	25	147	163	77,8	130,2	17	M16x50	5/8"-11x2"	
35	35	127	5"	BFX-311-CP	25	180	184	92	152,4	17	M16x55	5/8"-11x2"1/4	

#### 4.8 Universal Joint specifications

The hydraulic actuator is attached to a saddle and block through universal joints so as to allow the necessary relative movement as discussed in section 3.3 and shown in Figure 3.6. A drawing of a universal joint is shown along with 3-D preview in Figure 4.21

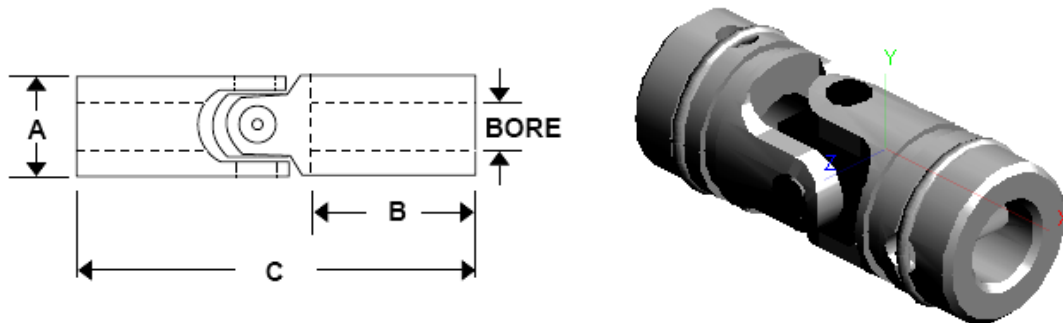


**Figure 4.21 Drawing along with 3-D preview of a universal joint**

The specifications for the universal joint were found in the catalog of a Pennsylvania-based company named Rush Gears. To attach the joint on the rod of the actuator the rod diameter has to be matched with the bore diameter of the universal joint.

Rod diameter is 3.0 inches (76.2mm). According to the product catalog, the maximum bore diameter for a universal joint was of 2.00 inches. While searching for the particular universal joint, it was observed that standard size for a universal joint goes upto 2 inches bore diameter. The next size available in the market was one with bore diameter of 6.00 inches which seems to be unreasonable to be used here in this application. However, a customized order can be placed with many companies, Rush Gears being one of them. For a universal joint with a bore diameter of 3.0 inches, the other specifications will roughly look like as summarized in the Table 4.7. The universal joint on other side is attached to the saddle.

**Table 4.7 Estimated specifications for a 3” bore diameter universal joint**

Bore Dia.		Outside Diameter, A		Hub Length, B		Overall Length, C		Approx Weight	
inch	mm	inch	mm	inch	mm	inch	mm	lbs	Kg
3	76.2	4.85	123.2	3.7	94	13.2	335.3	59	26.76

The universal joint is attached to the blind flange on one end and to the block at the other end. To have enough space for the universal joint to fit on the block, the face of the block has to be greater than the outer diameter of the universal joint, which is 123.2mm. So, the face of the block will be a square of 200mm x 200mm as shown in Figure 4.22. This solid block is made of mild steel.

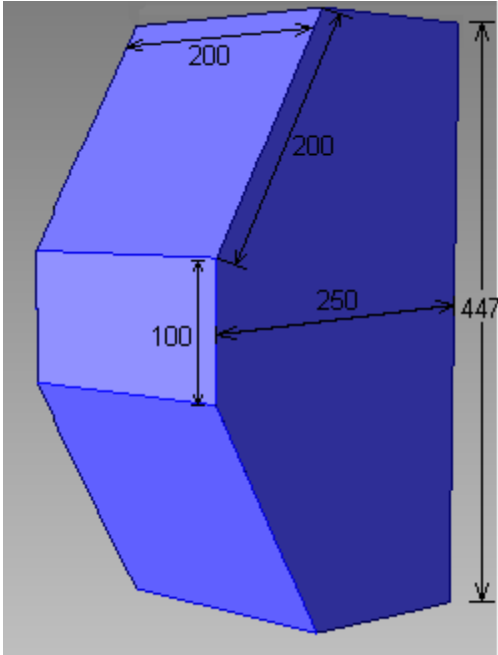


**Figure 4.22 Drawing specifications for the block**

Volume of this block comes out to be  $9420 \text{ cm}^3$ . Density of mild steel is  $7.85 \text{ g/cm}^3$ . Hence, the weight of block comes out to be  $74 \text{ Kg}$  (~163 pounds)

#### **4.9 Linear guide rail system requirements**

Linear guide rail system is attached to the saddle on the blade at 70% station where the flap deflection was calculated to be 2.82m. The first flap frequency is 0.365Hz. The motion of the flap can be described as a sinusoidal wave with amplitude of 2.82m and a frequency of 0.365Hz, for which the equation of motion looks like

$$X = A \sin (2\pi f t), \text{ where}$$

$X$  = displacement of the blade at 70% station in the vertical direction,

$A$  = amplitude, or flap deflection

$f$  = frequency,

$t$  = time (in seconds)

Based on these requirements, the company named “Schaeffler” was contacted which provided the relevant product information and a price quote. The information about the four-row linear recirculating ball bearing and guideway assemblies provided by the company can be found in Appendix 1. As per the recommendation made by the company’s application engineer, for preparing this concept, size 55, long style carriages would be the best to use here for this application. A rough estimate of what a distributor would charge is \$450 per bearing and \$2100 for a 3200 mm long rail making it a total of \$6000.

The vertical post to floor, also referred to as carriage is an I-beam, available in numerous variants. They have saddle plates with hardened and precision ground rolling element raceways. The slider or guideway is made from hardened steel and is ground on all the faces.

#### **4.9.1 Active trolley system**

The guide rail system needs another means by which it can move up and down along with the flapwise motion of the blade. If the guide rail assembly is allowed to move on its own, the B-rex system has to apply much greater force taking the weight of the hydraulic actuators, universal joints and guide rails assembly into consideration. The one way to resolve this is to attach another hydraulic actuator which moves the guide rail assembly up and down simultaneously with the flapwise motion of the blade. For the design requirements of this hydraulic actuator, we need to know the force required to be delivered acting against the mass of the guide rail assembly, weight of the hydraulic actuators and the force of friction in the guide rail bearings.

#### 4.9.2 Force to be delivered by hydraulic actuator

A bearing weighs 6 kg and the guideway weighs 13.3 kg per meter of length. Now looking at the dimension table of guideway assemblies for the series 55 [Appendix 1], we have a maximum length of 2520 mm. So the total guide rail system including the four bearing would weigh around 57.52 kg or 127 pounds ( $6 \text{ kg} * 4 + 13.3 \text{ kg} * 2.52$ ). Also, the force of friction in the guide rail system is 66N per bearing making it a total of 264N. The hydraulic actuator series 201.30 with a 70-inch stroke length would weigh around 454 kg or 1000 pounds.

So also taking the weight of universal joint into consideration, we can design the hydraulic actuator for the vertical motion of the linear guide rail system. The flapwise frequency of the blade comes out to be 0.365Hz (ref. Table 4.2) and the distance traveled by blade in vertical direction at 70% of its length is 2.8m. The equation governing the vertical motion can be written as,

$$X = A \sin(2\pi ft),$$

Here amplitude,  $A = 2.8/2 = 1.6\text{m}$

Frequency,  $f = 0.365\text{Hz}$

$$\text{Now we have, } \ddot{X} = -(2\pi f)^2 A \sin(2\pi ft)$$

So, the maximum acceleration,  $\ddot{X}_{\max} = (2\pi f)^2 A = (2 * \pi * 0.365)^2 * 1.4 = 7.36\text{m/s}^2$

The maximum force acting vertically against which the hydraulic actuator has to work is the weight of two inclined actuators, and the block, the weight of the linear guide rail system, the force of friction acting between the four row linear bearing assembly and the maximum acceleration in the whole system.

The maximum force acting in the vertical direction =  $(mg+ma) + \text{frictional force}$ , where 'm' is the total mass of the linear actuators, linear guide rail system and universal joints, which comes out to be 1050 kg or 2310 pounds. So the maximum force =  $1050(9.8+7.36) + 264 = 18282\text{N} \sim 18.3\text{kN}$

To serve the purpose, we need a hydraulic actuator with a  $\sim 3\text{m}$  stroke length. Now, for a hydraulic actuator, a stroke length of  $3\text{m}$  is quite large and is not commonly available in the market and hence needs to be custom engineered. The company named MTS, as mentioned earlier also in the report was contacted to get a rough estimate of the cost and product specification. As this will be a custom designed product, it was not able to get the specific details but a hydraulic actuator with  $25\text{kN}$  force rating can be used for the purpose delivering a stroke of  $3\text{m}$  at a frequency of  $0.365\text{ Hz}$ . The flow rate required here will be  $50\text{gpm}$  and the cost of the actuator will be roughly  $\$150,000$ .

## CHAPTER 5

### CONCLUSION

Hybrid testing and forced-displacement testing of wind turbines blades in the edgewise direction require a means of forcing the blade displacement in the edgewise direction. During the past 10 years of testing, NREL has used a bell crank system to impart this displacement. However, NREL's experience with the NREL bell crank system is limited to blades less than 40m long. It is expected that customers will request that dual axis testing in some form be performed at the large blade test facilities on larger blades.

The conventional bell crank systems previously used by NREL to perform dual-axis testing are likely to be expensive due to the lateral space requirements (push rod length) and system mass required to sufficiently mitigate the flap/edge coupling and induced pitch moment. One alternative is an Actively-positioned Bell Crank system (ABC). Although this concept addresses the induced pitch problem, an ABC may not sufficiently reduce the lateral space required for a bell crank system. Using a passive trolley system with two inclined edgewise actuators, mounted via universal joints allows the blade to be significantly closer to the trolley rail, proportionally reducing pitch moments imparted by the system mass and trolley friction. The kinematics of the design was proved to be working by making conceptual model in SolidWorks.

A hydraulic system configured for this application would require actuators, hydraulic power units (HPU), control system, hydraulic distribution, fixturing and engineering support which will cost around \$1.4 million. Linear guide rail system would

use four-row linear recirculating ball bearing and guideway assemblies which will cost around \$6000, which is negligible as compared to \$1.4 million. The cost for building this system is more than the systems being used today; however, it is a more efficient and better way to test the large wind turbine blades. Instead of testing the blade in flapwise and edgewise direction separately for months, this design is capable of testing the blades in both directions at the same time. This will reduce the testing time by 50%. It is highly recommended to build this design to test large wind turbine blades in order to test them more efficiently and in much lesser period of time.



## **CHAPTER 6**

### **FUTURE WORK**

The blade-mounted edgewise excitation system requires dramatically less space and can potentially eliminate the flap/edge coupling and pitch problems, but significant development challenges remain. One challenge is that a trolley bearing system must be identified or developed capable of very high loads and relatively fast speeds (averaging up to 6 m/s or 13 mph) continuously reversed having a displacement of 3m. On the other hand, large displacement is good as it reduces the force required. A second challenge is that a control system must be developed for the actuation systems that ensures the trolley stays vertically aligned with the blade (to avoid flap/edge coupling) and imparts the desired pitch moment. One more challenge is the complication involved with custom engineered hydraulic actuator with a 3m long actuator stroke. Other unexpected challenges may arise during implementation of this approach. For example, the simplified schematics displayed in this report do not address how factors such as out-of-plane loads will affect the saddle attachment to the blade.

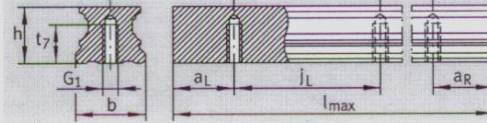
The alternative design which is brought up in this report has been designed in SolidWorks to confirm the kinematics of the model and the system requirements including hydraulic system, linear guide rail system, flange joint, universal joint specifications are described. The future work may include designing a prototype for this model.

## APPENDIX A

### LINEAR GUIDEWAY ASSEMBLY SPECIFICATION CHART

#### Four-row linear recirculating ball bearing and guideway assemblies

Full complement  
Standard, L, N and NL carriages



172 338a

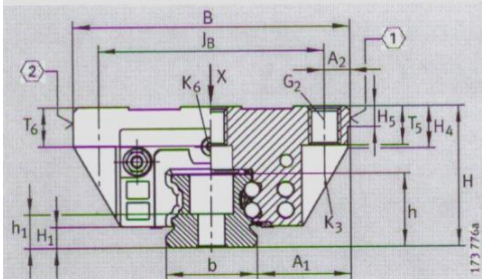
TKVD...U

Dimension table · Dimensions in mm

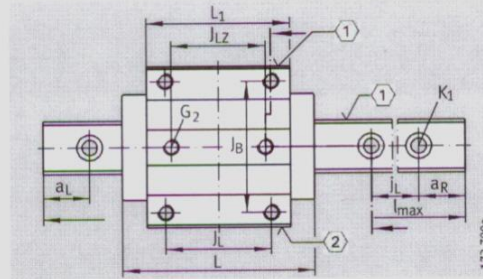
Designation	Dimensions				Mounting dimensions											
	l <sub>max</sub> <sup>1)</sup>	H	B	L	A <sub>1</sub>	J <sub>B</sub>	b	A <sub>2</sub>	L <sub>1</sub>	J <sub>L</sub>	J <sub>LZ</sub>	J <sub>L</sub>	a <sub>L</sub> , a <sub>R</sub> <sup>2)</sup>		H <sub>1</sub>	H <sub>4</sub>
													min.	max.		
KUVE15-B	1200	24	47	59,6	16	38	15	4,5	39,8	30	26	60	20	53	4,3	7,6
KUVE20-B	2960	30	63	69,8	21,5	53	20	5	50,4	40	35	60	20	53	4,5	11
KUVE20-B-L				87,3												
KUVE20-B-N		69,8	50,4													
KUVE20-B-NL		87,3	67,9													
KUVE25-B	2960	36	70	81,7	23,5	57	23	6,5	60,7	45	40	60	20	53	5,1	10,9
KUVE25-B-L				107,5					86,5							
KUVE25-B-N		81,7	60,7													
KUVE25-B-NL		107,5	86,5													
KUVE30-B	2960	42	90	97,4	31	72	28	9	72	52	44	80	20	71	5,9	13,8
KUVE30-B-L				125,4					100							
KUVE30-B-N		97,4	72													
KUVE30-B-NL		125,4	100													
KUVE35-B	2960	48	100	110,4	33	82	34	9	80	62	52	80	20	71	6,7	14,3
KUVE35-B-L				143,4					113							
KUVE35-B-N		110,4	80													
KUVE35-B-NL		143,4	113													
KUVE45-B	2940	60	120	139	37,5	100	45	10	102,5	80	60	105	20	94	9,7	19,9
KUVE45-B-L				171,1					134,6							
KUVE45-B-N		139	102,5													
KUVE45-B-NL		171,1	134,6													
KUVE55-B	2520	70	140	172	43,5	116	53	12	132	95	70	120	20	107	13,5	22,7
KUVE55-B-L				210					170							

For further table values, see page266 and page267.

- 1) Maximum length of single-piece guideways. For permissible number of guideway pieces, see page259.  
Maximum single-piece guideway length of 6 m available by agreement.
- 2) a<sub>L</sub> and a<sub>R</sub> are dependent on the guideway length.
- 3) If there is a possibility of preload loss due to settling, the fixing screws should be secured against rotation.
- 4) (1) Locating face  
(2) Marking

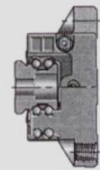


KUVE..-B (-L, -N, -NL)  
①, ②<sup>4)</sup>



KUVE..-B (-L, -N, -NL) · View rotated 90°  
①, ②<sup>4)</sup>

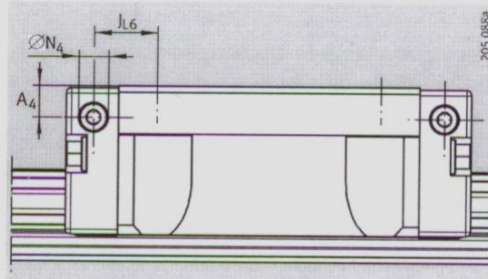
											Fixing screws <sup>3)</sup>							
H <sub>5</sub>	T <sub>5</sub>	T <sub>6</sub>	t <sub>7</sub>	h	h <sub>1</sub>	G <sub>1</sub>		G <sub>2</sub>		K <sub>1</sub>		K <sub>3</sub>		K <sub>6</sub>		K <sub>6</sub>		
						DIN ISO 4762-12.9												
						M <sub>A</sub>	M <sub>A</sub>	M <sub>A</sub>	M <sub>A</sub>	M <sub>A</sub>	M <sub>A</sub>	M <sub>A</sub>	M <sub>A</sub>	M <sub>A</sub>	M <sub>A</sub>	M <sub>A</sub>	M <sub>A</sub>	
						Nm	Nm	Nm	Nm	Nm	Nm	Nm	Nm	Nm	Nm	Nm	Nm	
4,75	7	5,8	8	15	8,15	M5	10	M5	5,8	M4	5	M4	5	-	-	M4	2	
5,25	10	7,5	10	17	9,1	M6	17	M6	10	M5	10	M5	10	M5	10	M5	10	-
	8	6											-	-	M5	4		
5,25	10	10	12	18,7	8,7	M6	17	M8	24	M6	17	M6	17	M6	17	-	-	
		8											-	-	M6	8		
6,25	12	11,5	15	23,5	11,5	M8	41	M10	41	M8	41	M8	41	M8	41	-	-	
		9											-	-	M8	12		
6,75	13	12,3	15	27	15	M8	41	M10	41	M8	41	M8	41	M8	41	-	-	
		8,3											-	-	M8	12		
9,25	15	15	20	34,2	16,2	M12	140	M12	83	M12	140	M10	83	M10	83	-	-	
		11											-	-	M10	35		
11,25	21	18	22	41,5	19,5	M14	220	M14	140	M14	220	M12	140	M12	140	-	-	





## Four-row linear recirculating ball bearing and guideway assemblies

Full complement  
Standard, L, N and NL carriages

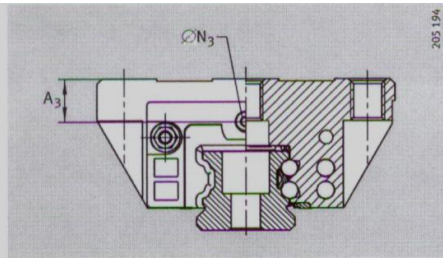


Lubrication connector on lateral face

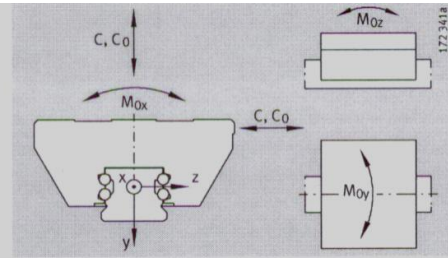
Dimension table (continued) · Dimensions in mm

Designation	Carriage		Guideway		
	Designation	Mass m ≈ kg	Designation	Mass m ≈ kg/m	Closing plug K <sub>2</sub>
KUVE15-B	KWVE15-B	0,2	TKVD15-B (-U) <sup>2)</sup>	1,44	KA07-TN/A
KUVE20-B	KWVE20-B	0,44	TKVD20 (-U)	2,2	KA10-TN/A
KUVE20-B-L	KWVE20-B-L	0,59			
KUVE20-B-N	KWVE20-B-N	0,37			
KUVE20-B-NL	KWVE20-B-NL	0,51			
KUVE25-B	KWVE25-B	0,68	TKVD25(-U)	2,7	KA11-TN/A
KUVE25-B-L	KWVE25-B-L	1			
KUVE25-B-N	KWVE25-B-N	0,56			
KUVE25-B-NL	KWVE25-B-NL	0,82			
KUVE30-B	KWVE30-B	1,2	TKVD30(-U)	4,3	KA15-TN/A
KUVE30-B-L	KWVE30-B-L	1,7			
KUVE30-B-N	KWVE30-B-N	1			
KUVE30-B-NL	KWVE30-B-NL	1,5			
KUVE35-B	KWVE35-B	1,75	TKVD35(-U)	5,7	KA15-TN/A
KUVE35-B-L	KWVE35-B-L	2,52			
KUVE35-B-N	KWVE35-B-N	1,56			
KUVE35-B-NL	KWVE35-B-NL	2,23			
KUVE45-B	KWVE45-B	3,3	TKVD45(-U)	9,2	KA20-TN/A
KUVE45-B-L	KWVE45-B-L	4,3			
KUVE45-B-N	KWVE45-B-N	2,72			
KUVE45-B-NL	KWVE45-B-NL	3,38			
KUVE55-B	KWVE55-B	5,5	TKVD55-B(-U)	14	KA24-TN/A
KUVE55-B-L	KWVE55-B-L	6,6			

- 1) Calculation of basic load ratings in accordance with DIN636.  
Based on practical experience, it may be possible to increase the basic dynamic load rating.
- 2) The new carriages cannot be used on the previous guidewaysTKVD15(-U).
- 3) Tapered head lubrication nipple to DIN71 412-BM6,  
KUVE20-B to DIN71 412-BM5 and KUVE15-B to DIN3405-BM3, supplied loose with delivery.
- 4) Maximum permissible screw depth for lubrication connectors.

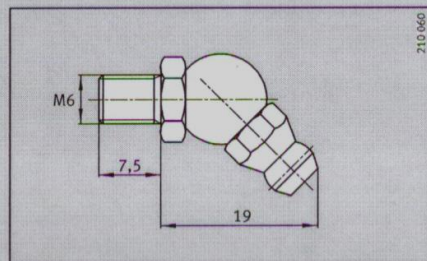
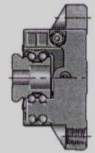


Lubrication connector on end face

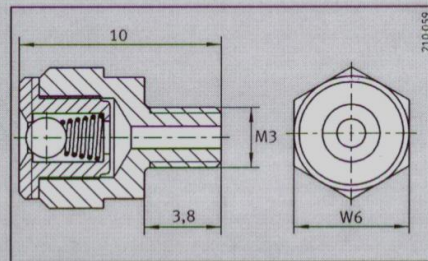


Load directions

Dimensioning of lubrication connectors						Load carrying capacity <sup>1)</sup>					
$A_3$	$\varnothing N_3$		$A_4$	$\varnothing N_4$		$l_{L6}$	Basic load ratings		Moment ratings		
		<sup>4)</sup>			<sup>4)</sup>		C N	$C_0$ N	$M_{Ox}$ Nm	$M_{Oy}$ Nm	$M_{Oz}$ Nm
4,3	2,57	5,5	3,2	2,57	5,5	9,1	7200	14500	150	100	100
7,7	4,5	7	4,6	4,5	5,5	9,4	13100	27000	332	240	240
			18,9	16200		36500	452	430	430		
4,7			3,3	2,57		9,4	13100	27000	332	240	240
			18,9	16200		36500	452	430	430		
11	5,5	7	6,5	5,6	7	12,85	17900	37000	510	395	395
			25,75	23400	54000	745	825	825			
6			4	2,57	6	12,05	17900	37000	510	395	395
			24,95	23400	54000	745	825	825			
11,5	5,5	7	7	5,5	7	15,5	27500	55000	970	660	660
			29,5	34500		74000	1320	1180	1180		
7,5			4,95	4,5		15,1	27500	55000	970	700	700
			29,1	34500		74000	1310	1240	1240		
12,3	5,5	7	11	5,5	7	16	38000	72000	1465	1020	1020
			32,5			47500	100000	2625	1890	1890	
8,3			7			16	38000	72000	1465	1020	1020
			32,5			47500	100000	2025	1890	1890	
16,5	5,5	7	16,5	5,5	7	19,25	69000	141000	3610	2485	2485
			35,3			82000	181000	4635	4000	4000	
8,5			8,5			19,25	69000	141000	3610	2485	2485
			35,5			82000	181000	5635	4000	4000	
15	5,5	7	15	5,5	7	30,5	104000	213000	5600	2730	2730
			49,5			127000	285000	7500	4725	4800	



Lubrication nipple<sup>3)</sup>



Lubrication nipple<sup>3)</sup>,  
width across flat  $W=6\text{mm}$

## APPENDIX B

### MATLAB INPUT FILES

<b>Blade Data</b>							
input blade data as given from the blade manufacturer (if certain information is unknown place a zero as the first value) - length of data does not matter							
<b>Blade Name</b>							
61.33m Blad (name must be limited to three words)							
<b>Number of Input Blade Data Points</b>							
49							
Station (m)	MPL (kg/m)	Chord (m)	Twist (deg)	Flap EI (N*m <sup>2</sup> )	Edge EI (N*m <sup>2</sup> )	GJ (N*m <sup>2</sup> )	EA (N*m <sup>2</sup> )
0	678.935	3.3581	13.308	1.81E+10	1.81E+10	5.56E+09	1.39E+10
0.1993225	678.935	3.5006	13.308	1.81E+10	1.81E+10	5.56E+09	1.39E+10
1.1965483	773.363	3.6433	13.308	1.80E+10	1.96E+10	5.43E+09	1.51E+10
2.1937741	740.55	3.7862	13.308	1.75E+10	1.95E+10	4.99E+09	1.37E+10
3.1909999	740.042	3.9293	13.308	1.53E+10	1.98E+10	4.67E+09	1.33E+10
4.1882257	592.496	4.0727	13.308	1.08E+10	1.49E+10	3.47E+09	9.98E+09
5.1854515	450.275	4.2194	13.308	7.23E+09	1.02E+10	2.32E+09	6.89E+09
6.1826773	424.054	4.3902	13.308	6.31E+09	9.14E+09	1.91E+09	6.05E+09
7.1799031	400.638	4.5283	13.308	5.53E+09	8.06E+09	1.57E+09	5.28E+09
8.1783555	382.062	4.5856	13.308	4.98E+09	6.88E+09	1.16E+09	4.46E+09
9.1743547	399.655	4.6238	13.308	4.94E+09	7.01E+09	1.00E+09	4.33E+09
10.1715805	426.321	4.6472	13.308	4.69E+09	7.17E+09	8.56E+08	4.46E+09
11.1688063	416.82	4.6482	13.181	3.95E+09	7.27E+09	6.72E+08	4.63E+09
12.1660321	406.186	4.6013	12.848	3.39E+09	7.08E+09	5.47E+08	5.02E+09
13.1644845	381.42	4.5261	12.192	2.93E+09	6.24E+09	4.49E+08	4.37E+09
14.1604837	352.822	4.4543	11.561	2.57E+09	5.05E+09	3.36E+08	3.48E+09
15.1577095	349.477	4.3926	11.072	2.39E+09	4.95E+09	3.11E+08	3.26E+09
16.1549353	346.538	4.3294	10.792	2.27E+09	4.81E+09	2.92E+08	3.03E+09
18.1506135	339.333	4.2636	10.232	2.05E+09	4.50E+09	2.61E+08	2.56E+09
20.1444518	330.004	4.1938	9.672	1.83E+09	4.24E+09	2.29E+08	2.17E+09
22.1389034	321.99	4.1202	9.11	1.59E+09	4.00E+09	2.01E+08	1.88E+09
24.133355	313.82	4.0445	8.534	1.36E+09	3.75E+09	1.74E+08	1.62E+09
26.1278066	294.734	3.9676	7.932	1.10E+09	3.45E+09	1.44E+08	1.25E+09
28.1228715	287.12	3.8881	7.321	8.76E+08	3.14E+09	1.20E+08	1.02E+09
30.1167098	263.343	3.808	6.711	6.81E+08	2.73E+09	8.12E+07	7.59E+08
32.1111614	253.207	3.7301	6.122	5.35E+08	2.55E+09	6.91E+07	6.59E+08
34.105613	241.666	3.6544	5.546	4.09E+08	2.33E+09	5.75E+07	5.56E+08
36.1000646	220.638	3.5798	4.971	3.15E+08	1.83E+09	4.59E+07	4.19E+08
38.0951295	200.293	3.5052	4.401	2.39E+08	1.58E+09	3.60E+07	3.42E+08
40.0889678	179.404	3.4301	3.834	1.76E+08	1.32E+09	2.74E+07	2.70E+08
42.0834194	165.094	3.355	3.332	1.26E+08	1.18E+09	2.09E+07	2.98E+08
44.077871	154.411	3.2799	2.89	1.07E+08	1.02E+09	1.85E+07	2.40E+08
46.0723226	138.935	3.2048	2.503	9.09E+07	7.98E+08	1.63E+07	1.77E+08
48.0680008	129.555	3.1297	2.116	7.63E+07	7.10E+08	1.45E+07	1.46E+08
50.0612258	107.264	3.0546	1.73	6.11E+07	5.18E+08	9.07E+06	9.68E+07
52.0556774	98.776	2.9795	1.342	4.95E+07	4.55E+08	8.06E+06	7.96E+07
54.050129	90.248	2.9044	0.954	3.94E+07	3.95E+08	7.08E+06	6.47E+07
55.0473548	83.001	2.8293	0.76	3.47E+07	3.54E+08	6.09E+06	5.49E+07
56.0445806	72.906	2.7542	0.574	3.04E+07	3.05E+08	5.75E+06	2.80E+07
57.0418064	68.772	2.6791	0.404	2.65E+07	2.81E+08	5.33E+06	2.51E+07
57.5404193	66.264	2.604	0.319	2.38E+07	2.62E+08	4.94E+06	2.22E+07
58.0402588	59.34	2.5289	0.253	1.96E+07	1.59E+08	4.24E+06	1.13E+07
58.5376451	55.914	2.4561	0.216	1.60E+07	1.38E+08	3.66E+06	8.61E+06
59.036258	52.484	2.3838	0.178	1.28E+07	1.19E+08	3.13E+06	6.44E+06
59.5348709	49.114	2.3021	0.14	1.01E+07	1.02E+08	2.64E+06	4.77E+06
60.0334838	45.818	2.2147	0.101	7.55E+06	8.51E+07	2.17E+06	3.40E+06
60.5320967	41.669	2.0949	0.062	4.60E+06	6.43E+07	1.58E+06	1.94E+06
61.0307096	11.453	1.8675	0.023	2.50E+05	6.61E+06	2.50E+05	3.80E+05
61.33	10.319	1.5159	0	1.70E+05	5.01E+06	1.90E+05	2.30E+05



## Saddle Data

<b>Saddle Data</b>						
input saddle data used for test (weights can be set to zero if unknown and code will optimize but locations must be given)						
<b>RTS Weight (N)</b>	<b>RTS Location (m)</b>					
10909	43					
<b>Number of Additional Saddles</b>						
2						
<b>Weight (N)</b>	<b>Location (m)</b>					
13519	31					
44549	52					

## Test Data

<b>Test Data</b>						
input parameters for dynamic fatigue test						
<b>Type of Test</b>						
1 = flapwise, 2 = dual-axis						
2						
<b>Number of Elements</b>						
49						
<b>Actuator Stroke (m)</b>						
the 15 kip MTS actuator has a maximum stroke of 0.254 m						
0.25						
<b>% Critical Damping</b>						
damping ratio (i.e. 1.1 = 1.1% = 0.011)						
0.474						
<b>Save Matlab Workspace Blade Name</b>						
describes the blade in one word (i.e. KnC26 or GE34)						
5MW-62m						

## REFERENCES

- [1] Manwell, J.F., McGowan, J., Rogers, T., “Wind energy Explained: Theory, Design and Application”, University of Massachusetts, Amherst, MA, 2002
- [2] Johnson, G., Wind Energy Systems, Prentice Hall, Englewood Cliffs, NJ, 1985.
- [3] Le Gourieres, D., Wind Power Plants, Pergamon Press, Oxford, 1982.
- [4] Nelson, V., Wind Energy and Wind Turbines, Alternative Energy Institute, Canyon, TX, 1996.
- [5] Hills, R., Power from Wind, Cambridge University Press, Cambridge, UK, 1994.
- [6] Inglis, D., Windpower and Other Energy Options, University of Michigan Press, Ann Arbor, MI, 1978.
- [7] Putnam, P., Power from the Wind, Van Nostrand Reinhold, New York, 1948.
- [8] Berger, J., Charging Ahead: The Business of Renewable Energy and What it Means for America, University of California Press, Berkley, CA, 1997.
- [9] Harrison, R., Hau, E., Snel, H., Large Wind Turbines: Design and Economics, Wiley Chichester, 2000.
- [10] White, D., “New Method for Dual-Axis Fatigue Testing of Large Wind Turbine Blades Using Resonance Excitation and Spectral Loading”, *NREL/TP-500-35268*, April 2004
- [11] World Cumulative Installed Wind Power Capacity and Net Annual Additions, 1980-2007, Source: [http://earth-policy.org/Indicators/Wind/2008\\_data.htm#fig1](http://earth-policy.org/Indicators/Wind/2008_data.htm#fig1)
- [12] Greuning, S.V., Idaho Energy Division / Courtesy of NREL)  
Source: <http://www.sciencedaily.com/releases/2007/05/070503110317.htm>
- [13] Technical Specification, Wind Turbine Generator Systems Part 23: Full scale structural testing of rotor blades, *International Electrotechnical Commission (IEC) report TS 61400-23*
- [14] NREL Picture, source: [www.nrel.gov/wind/news/2006/466.html](http://www.nrel.gov/wind/news/2006/466.html)
- [15] Cotrell, J., Malhotra, P., “Bell Crank specifications for 50-70m blades”, *Draft NREL Spreadsheet*, November 2008.



[16] Jason Cotrell, Scott Hughes, Puneet Malhotra, "Scoping of a dual-axis, forced displacement, Edgewise Actuator for testing 50-70m blades", *Draft NREL Report*, March 2009.

[17] Cotrell, J., Hughes, S., Desmond, M., White, D., "Finite Element modeling of a dual axis resonant system for wind turbine blades", Proceedings of ES2009-90164, Energy Sustainability 2009, July19-23, 2009, San Francisco, California, USA

[18] Jonkman, J., Butterfield, S., Musial, W., and Scott, G., "Definition of a 5-MW Reference Wind Turbine for Offshore System Development", NREL/TP-500-38060, Golden, CO: National Renewable Energy Laboratory, February 2009.

[19] Available online:

[[www.webcoindustries.com/tubing/mechanical/sizechartdrawntube.cfm](http://www.webcoindustries.com/tubing/mechanical/sizechartdrawntube.cfm)]

[20] Available online:

[[www.stauff.com/fileadmin/Downloads/PDF/Fluid\\_Connectors/SAE-Flanschkatlog\\_07-2009.pdf](http://www.stauff.com/fileadmin/Downloads/PDF/Fluid_Connectors/SAE-Flanschkatlog_07-2009.pdf)]

[21] The MathWorks, 2008, "fmincon," Optimization Toolbox, MathWorks Inc., Natick, Massachusetts, United States.

[22] Desmond, M., "The Development of a Wind Turbine Blade Finite Element Model to Predict Loads and Deflections during Static and Fatigue Structural Testing", December 16, 2009, Embry-Riddle Aeronautical University, Daytona Beach, FL.

[23] R. Nagle, E. Saff, and A. Snider, 2004, "Fundamentals of Differential Equations," Sixth Edition, Pages 123-138, Pearson Education, United States.

[24] D. Samborsky, and J. Mandell, 2008, "DOE/MSU Composite Material Fatigue Database," Version 17.0, Montana State University, Chemical and Biological Engineering Department, Bozeman, Montana, United States.

[25] H. Sutherland, and J. Mandell, "Updated Goodman Diagrams for Fiberglass Composite Materials," Sandia National Laboratories, Albuquerque, New Mexico, United States.